

University of Southern Queensland
Faculty of Health, Engineering & Sciences

**Simulation of the Effects of Wind on the Drag on Kayakers in
Competition**

A dissertation submitted by

D. Long

in fulfilment of the requirements of

ENG4112 Research Project

towards the degree of

Bachelor of Mechanical Engineering (Honours)

Submitted: October, 2020

Abstract

This project applies an understanding of fluid mechanics to study the effects of wind on kayakers in competition using computational fluid dynamic software. A multiphase model was created on ANSYS Fluent to simulate the flow conditions and find the drag outputs. The model includes two inlets, to allow for separate air and water velocities, and uses a volume of fluid multiphase system with an SST $k - \omega$ turbulence model. Kayaker velocities from 1-7m/s are combined with relative headwinds from 1-10m/s to determine the hydrodynamic and aerodynamic drag due to windy conditions. The wind stress on the water's surface is also simulated through small waves included in the boundary conditions. The results found an exponential increase of drag of approximately $D_F = 2.15\vec{V}^2 - 6.47\vec{V} + 5.43$ as a function of velocity in static air conditions. For a kayaker at racing pace facing a maximum 10m/s headwind, the results show a drag increase of approximately 5%, decreasing as kayak velocity increased. The largest components of drag for a kayaker are the hydrodynamic skin friction and wave drag, hence the low air drag percentage was expected relative to the dominant hydrodynamic drag. The drag due to small waves on the water's surface was found to range from 5-6% at race pace, and was considered to have the larger effect on competitors, as wind speeds from 8-10m/s are very high and unlikely during competition. The model was used to compare the drag of common racing strategies, and findings suggests that an even-pacing requires less energy than the commonplace "reverse J" strategy. There were some limitations to the research project involving software and time constraints, and further work recommendations are made in the report which suggest refinements and future applications of the model.

ENG4111/2 *Research Project*

Limitations of Use

The Council of the University of Southern Queensland, its Faculty of Health, Engineering & Sciences, and the staff of the University of Southern Queensland, do not accept any responsibility for the truth, accuracy or completeness of material contained within or associated with this dissertation.

Persons using all or any part of this material do so at their own risk, and not at the risk of the Council of the University of Southern Queensland, its Faculty of Health, Engineering & Sciences or the staff of the University of Southern Queensland.

This dissertation reports an educational exercise and has no purpose or validity beyond this exercise. The sole purpose of the course pair entitled “Research Project” is to contribute to the overall education within the student’s chosen degree program. This document, the associated hardware, software, drawings, and other material set out in the associated appendices should not be used for any other purpose: if they are so used, it is entirely at the risk of the user.

Dean

Faculty of Health, Engineering & Sciences

Certification of Dissertation

I certify that the ideas, designs and experimental work, results, analyses and conclusions set out in this dissertation are entirely my own effort, except where otherwise indicated and acknowledged.

I further certify that the work is original and has not been previously submitted for assessment in any other course or institution, except where specifically stated.

D. LONG



Acknowledgments

I would like to begin by thanking my supervisors, Assoc Prof Andrew Wandel and Dr Khalid Saleh, for their assistance at important times throughout the project. I feel fortunate to have had the assistance of two experts in my research area, and the feedback provided to me was a big help. Many others from the teaching staff deserve recognition, for their assistance in preparing me for this project over my USQ experience.

Thanks also to my peers who have completed their Research Projects at the same time as me. It was always reassuring to know that the struggles I faced weren't uniquely mine. Finally, I would like to thank my family and friends, who I have had to sacrifice time with to achieve these goals. Their support was key to finishing this project.

D. LONG

Contents

Abstract	i
Acknowledgments	iv
List of Figures	xi
List of Tables	xiv
Chapter 1 Introduction	1
1.1 Background	1
1.2 Motivation	2
1.3 Project Goals	3
1.4 Overview of the Dissertation	4
Chapter 2 Literature Review	5
2.1 Chapter Overview	5
2.2 Competitive Kayaking	5
2.2.1 Energy Output	6

2.3	Kayak Dynamics	6
2.3.1	Hydrodynamics	8
2.3.2	Aerodynamics	8
2.3.3	Water Surface Waves	9
2.3.4	Open Channel Flow	9
2.3.5	Shallow Water Equations	10
2.3.6	Kelvin Ship Waves	11
2.4	Drag	12
2.4.1	Pressure Drag	12
2.4.2	Friction Drag	13
2.4.3	Lift-Induced Drag	14
2.4.4	Wave Drag	14
2.5	Dimensionless Numbers	15
2.5.1	Reynolds Number	15
2.5.2	Froude Number	16
2.5.3	Drag Coefficient	17
2.5.4	Bejan Number	17
2.6	Computational Fluid Dynamics	18
2.6.1	Transport Equations	19
2.6.2	Navier Stokes Equations	20

2.6.3	Meshing	20
2.6.4	RANS Turbulence Models	22
2.6.5	Multiphase Models	24
2.6.6	Volume of Fluid Method	25
2.6.7	CFD Solvers	26
2.7	Chapter Summary	26
Chapter 3 Methodology		27
3.1	Chapter Overview	27
3.2	FLUENT Workspace	27
3.3	Preliminary Simulations	29
3.3.1	Basic Wind Simulation	29
3.3.2	Wind around Cylinder Simulation	30
3.3.3	Kayak with Single Boundary Inlet Simulation	31
3.4	Project Simulation	34
3.4.1	Scope	34
3.4.2	Geometry	35
3.4.3	Meshing	37
3.4.4	Model Selection	39
3.4.5	Turbulence Model	40
3.4.6	Boundary Conditions	40

3.4.7	Solver Settings	41
3.4.8	Drag Calculation Methods	44
3.5	Chapter Summary	45
Chapter 4 Results		46
4.1	Chapter Overview	46
4.2	Simulation Outputs	46
4.2.1	Convergence	47
4.2.2	yPlus Value	47
4.3	Project Simulation	48
4.3.1	No wind Results	48
4.3.2	Baseline Simulations	48
4.3.3	Low-speed with Headwind	51
4.3.4	Racing Velocities with Headwind	53
4.3.5	Racing Velocities with Headwind and Waves	56
4.4	Chapter Summary	58
Chapter 5 Discussion		59
5.1	Chapter Overview	59
5.2	Simulations Results	59
5.3	Geometry	60
5.4	Meshing	61

5.5	Wave Creation	62
5.6	Effects of Wind	62
5.7	Pacing Strategy	62
5.8	Chapter Summary	64
Chapter 6 Conclusions and Further Work		65
6.1	Conclusion	65
6.2	Further Work	66
6.2.1	Model Refinements	66
6.2.2	Wave Creation	67
6.2.3	Practical Testing	67
6.2.4	Expansion of Model	68
References		69
Appendix A Project Specification		73
A.1	Project Timeline	75
Appendix B Fluent Outputs		76
B.1	Fluent Workspace Schematic	77
B.2	Example of Parameter Set Output	82
B.3	Example of Post Processing Menu	83

List of Figures

1.1	Difference between Kayaking (left) and Canoeing (right) (<i>ICF: Kayak</i> 2020)	2
2.1	Components of Ship Resistance (<i>Ship Resistance</i> 2020)	7
2.2	Scheme of a ship wake (Fang, Yang & Shugan 2011)	11
2.3	Mechanism of Pressure Drag, with flow separation aft of plate (NuclearPower 2020)	13
2.4	Boundary Layer of an Object, accounting for Friction Drag (NuclearPower 2020) .	14
2.5	Froude number as Wave pattern Vs Speed (Vallis 2019)	16
2.6	Common 2D and 3D Meshes in ANSYS Fluent (<i>ANSYS</i> 2020)	21
2.7	Differences between Structured and Unstructured Meshes (Versteeg & Malalaseker 2007)	22
3.1	ANSYS Workbench Schematic	28
3.2	Basic Model of Wind through a domain, with Inlet (blue) and Outlet (red)	29
3.3	Basic Model of Wind through a domain, with Inlet (forward) and Outlet (aft) . . .	30
3.4	Model of Wind around a Cylinder, with inlet (blue) and outlet (red)	31
3.5	Model of Air Flow around a Cylinder showing changes in velocity	31

3.6	Multifluid Model of Kayak with volume region wireframe shown centrally	33
3.7	Water Velocity around a Kayak Moving through Water	33
3.8	Geometry representing Kayaker	35
3.9	Geometry of Project Domain	36
3.10	Other Geometry Features	36
3.11	Wide View of the Mesh	37
3.12	Close View of the Mesh around the kayaker	38
3.13	Model after conversion to Polyhedral Mesh	39
3.14	Volume Fraction of water after initialisation, red indicating water.	40
3.15	Fluent Menu Settings	41
3.16	Convergence settings for the simulation	43
3.17	Calculation settings for the simulation	43
3.18	Drag Calculation Method found in post processing.	44
4.1	Typical Residual Report for Simulations	47
4.2	Contour of Yplus for 6m/s, ranged from 10 - 3000	48
4.3	Vector of the water's surface, showing change in velocity.	49
4.4	Drag Force Vs Kayak Speed - No Wind present.	49
4.5	Volume Rendering of the Velocity of fluids for a 1m/s and 5m/s kayaker	50
4.6	Air Velocity changes shown with Vectors for 5m/s velocity air.	50
4.7	Drag Force Vs Headwind Speed - Kayak Velocity 1m/s	52

4.8	Drag Force Vs Headwind Speed - Kayak Velocity 2m/s	53
4.9	Drag Force Vs Headwind Speed - Kayak Velocity 3m/s	53
4.10	Drag Force Vs Headwind Speed - Kayak Velocity 4m/s	55
4.11	Drag Force Vs Headwind Speed - Kayak Velocity 5m/s	55
4.12	Drag Force Vs Headwind Speed - Kayak Velocity 6m/s	56
4.13	Drag Force Vs Headwind Speed - Kayak Velocity 7m/s	56
4.14	Small Wave Effect on Bow Wave created by Kayak	57
4.15	Small Wave Effect on Water Surface close to Kayak	57
4.16	Drag Comparison of Wave Effect Vs Flat water Simulations	58
5.1	Contour of Yplus for 6m/s	61
5.2	Comparison of Pacing Strategies for 2018 WC final	63

List of Tables

4.1	Drag Forces found with no wind applied to simulation	50
4.2	Drag Forces for a Kayaker at 1m/s with increasing headwinds	51
4.3	Drag Forces for a Kayaker at 2m/s with increasing headwinds	51
4.4	Drag Forces for a Kayaker at 3m/s with increasing headwinds	52
4.5	Drag Forces for a Kayaker at 4m/s with increasing headwinds	54
4.6	Drag Forces for a Kayaker at 5m/s with increasing headwinds	54
4.7	Drag Forces for a Kayaker at 6m/s with increasing headwinds	54
4.8	Drag Forces for a Kayaker at 7m/s with increasing headwinds	55
5.1	World Championship Final Times	62

Chapter 1

Introduction

1.1 Background

Indigenous watercraft have existed for thousands of years, with the earliest known canoes, found in the Netherlands, carbon dated to between 8040 and 7510 BC (Pinkerton 2017). Australia's indigenous people utilised bark canoes for fishing, hunting and travelling, with evidence of some variants being used in Queensland for over 8000 years (Florek 2012). Although these are some of the earliest extant artefacts, they are probably not the first constructed, with the first known humans to leave Africa 100,000 years ago likely travelling over water utilising vessels such as canoes or rafts (Pinkerton 2017). It is accepted that light watercraft are responsible for the early spread and diversification of the human race.

Kayaking is an evolution of the canoeing, with the main differences being the participant is seated and uses a double ended paddle, as shown in figure 1.1. The earliest kayaks were used by the Greenland indigenous Inuit people up to 8000 years ago (*Kayak* 2020), and the word “ki ak” can be translated to “man-boat” (*ICF: Kayak* 2020). Modern kayaks are primarily used for recreation or sport. Competitive kayaking is an Olympic event covering distances of 200m, 500m and 1000m as an individual or team sport of up to 4 people (*Kayak* 2020).



Figure 1.1: Difference between Kayaking (left) and Canoeing (right) (*ICF: Kayak 2020*)

1.2 Motivation

Sports engineering is a relatively new discipline which goes about applying sports science into competitive advantage for athletes. Taha et al. (2013) define sports science as the analysis of the motion, physiology, biomechanics and psychology of an athlete. Sports engineering uses this analysis in designing, developing and researching methods to improve performance. Some modern examples are: the full body swimming suits used to break multiple world records; the 'hotspot' and 'snicko' devices used in cricket to determine ball contact on the bat; and the vast aerodynamic improvements made in motor racing through wind tunnels and computational fluid dynamics. Kayaking is a sport which is well suited to improvement through sports science, as it is essentially the athlete who overcomes drag the best who will achieve the fastest time, either by effort or efficiency. The importance of sport and its role in society continues to evolve.

Athletes are some of the largest role models in society, and the social media age means that competitors are judged for their behaviours and values in the societal and sporting arenas. The sporting industry seeks to continuously improve in both arenas, and sports engineering offers performance enhancement. The behaviours and attitudes of athletes goes towards improvement of society, through the voice it provides for members of all genders, religions and races. The benefits to society are strengthened by increasing the standing of athletes through high performance.

1.3 Project Goals

High level athletic kayaking can often be determined by margins of victory as small as thousandths of a second, making kayaking an extremely competitive sport. The predominant improvements made to race times during the period of 1948-2000 were associated to changes in design, most apparent when the same athlete competed at two or more Olympics in different boat designs (Robinson et al. 2002).

The primary goal of this project is to create a better understanding of the effects of wind on a kayaker during motion. This understanding will be achieved through the creation of a Computation Fluid Dynamic simulation on ANSYS Fluent. By creating this simulation, the magnitude and direction of the wind, as well as the kayaker speed, can be adjusted to find the drag forces in any condition.

From this understanding, it is expected that insights into how sprint kayakers can create a competitive advantage through minimising drag force or appropriately expending energy at the correct times. This simulation should continue to serve as an easy method of testing different strategies for kayak racing.

To achieve the primary project goal, a number of sub goals were devised to establish feasibility and scope of the project. Ordered chronologically, they were:

1. Conduct research on the movement of the kayak through the water, investigating the underlying mechanics.
2. Research CFD methods and their applications, including turbulence models, solution methods and meshing requirements.
3. Create a simple model of a body of water, and determine the impact of wind upon the water's surface.
4. Create an object in the centre of the simulation, to investigate the drag coefficients and compare them to research and expected values.
5. Create a model of a kayak and recreate the simulations, analysing the drag values and comparing them to the expected results

6. Provide feedback on observations and method in which a kayaker can achieve better race times.

If time permits the following tasks could be undertaken to gain a deeper understanding of watercraft dynamics:

7. Determine the suitability of the simulation for other watercraft, such as canoes, boats or wakeboards.
8. Find the best pacing strategy from an efficiency standpoint, based on drag findings at various velocities.

1.4 Overview of the Dissertation

Chapter 1 introduces the background, scope and motivation of the project. Establishes the aims and provides the outline to achieve them.

Chapter 2 is a review of the literature, establishing the fluid dynamic principals of the kayak motion. It also examines the best methods to recreate a kayaking system within Computational Fluid Dynamics software.

Chapter 3 discusses the methodology of the project, and the steps taken to create the project. This section also determines the feasibility of using the selected software through preliminary simulations. The scope of the model is also discussed.

Chapter 4 contains the results of the simulations. The results identified the drag outputs and trends for velocities of water from 1-7m/s and relative headwinds from 1-10m/s.

Chapter 5 provides discussion on the simulations and the results. Some of the projects challenges and limitations are mentioned, as well as how the project can help provide competition advantage.

Chapter 6 concludes the dissertation, and outlines further research and work required in this space.

Chapter 2

Literature Review

2.1 Chapter Overview

A literature review was undertaken seeking understanding in kayak dynamics and how best to simulate its motion. All the applicable areas of research have been evaluated against the aims of the project, and related to kayaking where possible. Research areas of interest include fluid dynamics, simulation techniques and current strategies athletes use to obtain competitive advantage.

2.2 Competitive Kayaking

The official fastest time recorded for a 200m K1 Kayaking event is 33.38 secs (*ICF: Kayak 2020*), which equates approximately to an average speed over the course of 6m/s. Records are not strictly kept in sprint events due to the difference in course set up and conditions. For Kayaking events, the ICF (International Canoe Federation) requires the water depth to be at least 2 meters. After research, no set wind limits can be found for kayaking events, only the requirement that conditions are judged to be safe by event officials.

2.2.1 Energy Output

Michael et al. (2008) find that kayaking is a sport requiring a high aerobic energy supply, however both aerobic and anaerobic energy systems are important factors in successful performance. Aerobic energy rate is measured as $\dot{V}O_2$, which indicates how efficiently oxygen is transported to the muscles. A greater measurement of $\dot{V}O_2$ indicates a higher rate of oxygen to fuel the muscles, and supramaximal performance can be increased for sprint kayakers (Bishop et al. 2002). Anaerobic energy is that which is sourced within the body, and not from oxygen through breathing.

Bishop et al. (2002) states that consensus for racing strategy by kayaking athletes is to start fast before transitioning to an even pacing strategy. This all-out start method was found to produce a greater kayak ergometer performance than an even pacing strategy, with a greater $\dot{V}O_2$ max evident. Borges et al. (2013) refers to this as a reverse J strategy, and suggests the tactic may be related to oxygen kinetics, avoiding wash from competitor or provide a psychological advantage. Pendergast et al. (1989) states the paddling speed of a kayaker can be found as:

$$\vec{V} = \frac{\dot{E}}{C} \quad (2.1)$$

where \dot{E} is the sum of the rate of aerobic ($\dot{V}O_2$) and anaerobic energy (\dot{E}_{AN}), and C is the energy cost per unit distance. As evident from the formula, an increase in either the aerobic or anaerobic rates of energy will result in faster kayak speed. The energy cost per meter (C) will be a function of the drag forces which opposes the forward motion of the kayak.

Fleming et al. (2012) tested a group of 10 male international flat-water kayakers to validate ergometer usage. During on-water testing the study found that the peak output force for the group was 238 Newtons, with a mean stroke rate of 82 strokes per minute. The personal best time of the group for a 500m K1 kayak race was less than 110 seconds (the record is 95 seconds) which suggests the data is able to be related to competition level athletes.

2.3 Kayak Dynamics

Mantha et al. (2013) have found that race time is the critical measure of performance for competition kayakers, which is determined from the mean velocity during a race. The factors which

contribute to performance are the athlete’s physical active strength, technique and kayak rowing hydrodynamic performance (Mantha et al. 2013). During kayaking competition, the athlete has to increase paddling effort drastically to overcome the sharp increases in drag at higher velocities. The various components, and subcomponents, of ship resistance is shown in figure 2.1. Hydro-

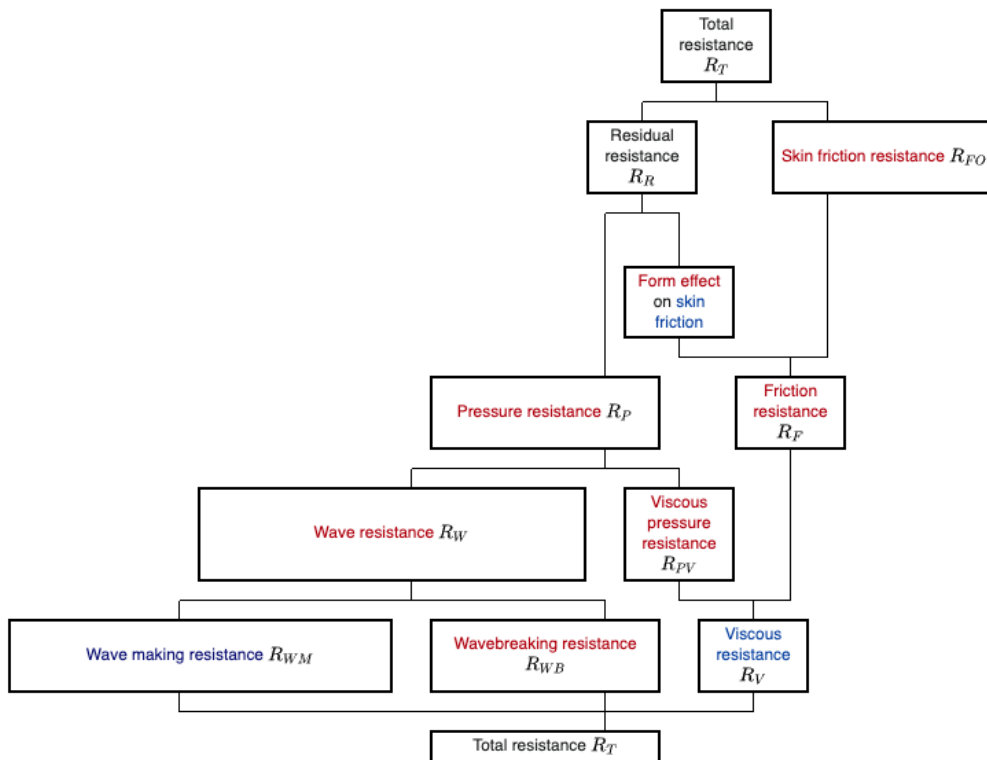


Figure 2.1: Components of Ship Resistance (*Ship Resistance* 2020)

dynamic research suggests that during low wind conditions approximately 93% of the drag on a canoe/kayak is the water, while the remaining 7% is created by the hull and the kayaker moving through the air above the water (Szanto 2014). This is due to the density of air being approximately 800 times less than water, subject to temperature and pressure. The simulation of the kayaker in competition requires interaction with two different fluids, water and air. The introduction of a second fluid increases the difficulty of the model and requires careful selection of model and solving settings. For a similar kayak CFD project, Barros (2015) summarises the system as a “two-phase, incompressible, isothermal flow, involving water and air, and the hull is assumed to have no translational or rotational motion aside from its forward velocity”.

2.3.1 Hydrodynamics

The motion of the kayak can be simplified to the force applied to the kayak through the athlete paddling, minus the drag forces of the water and air, with the resultant force a product of the mass and acceleration of the kayak/athlete system. Szanto (2014) estimates that the components of water resistant of a canoe being 2% frontal resistance, 80% surface friction, and 18% wave making resistance. These mechanisms were discussed in Section 2.4

Gomes et. al. (2017) categorises the types of hydrodynamic drag affecting the kayak hull into two types:

Frictional drag force: Depends solely on the Reynolds number and corresponds to the viscous forces. Also referred to as the skin friction drag (D_F), it can be simplified to the friction of the water on the hull. The mechanism causing frictional drag is explained in section 2.4.2.

Residual drag force: Depends exclusively on the Froude number, and contains the pressure drag (form drag) and wave-making resistance drag (wave drag). The pressure drag (D_{PR}) of the kayak can be summarised as the force required to move the water to form a path for the kayak. The wave drag (D_W) is the resistive force association with wave production (Gomes et. al. 2017).

The kayak's hydrodynamic performance is mainly dependent on hull geometrical shape, type of hull surface and weight of kayaker sitting in the boat (Gomes et al. 2017). It is generally accepted that the longer and slimmer the hull of a craft, the less pronounced the effect of friction will be (Canoe/Kayak: Hydrodynamics 2020), and modern designs are optimised by evolving to a narrowed hull with a decreased frontal and wetted surface area. The wetted surface area is critical as it determines D_F , and influences D_{PR} and D_W when combined with hull shape (Gomes et al. 2017).

2.3.2 Aerodynamics

Aerodynamic drag on a kayaker is caused by two mechanisms; the kayakers self-generated forward motion, and the local atmospheric boundary layer (ABL) winds (Barber 2018). The variables of the kayaker affecting the drag are the shape of the athlete, his/her form while kayaking and the

form of the kayakers equipment and apparel during motion.

2.3.3 Water Surface Waves

As an object moves on a free surface, a pattern of surface waves will appear, caused as a result of the kinetic energy transferred to the fluid by the object and the potential energy of the Earth's gravitational pull (Barros 2015). The force imparted by the wind on a body of water is also a cause of surface waves. Pelikan & Markova (2013) offer the cause of the wind waves as the surface stress imparted by the wind. For estimating the wind speed over water, they reference the formula:

$$U_{water} = 1.62 + 1.17U_{land} \quad (2.2)$$

where the air-water temperature difference does not exceed 5°C. From this, one proposed equation for the drag coefficient, subject to elevation and stability, can be found as:

$$C_D = 0.001(1.1 + 0.035U_{10}) \quad (2.3)$$

where U_{10} is the wind speed at 10 meters. Finally, from this, the stress imparted on the water is found as:

$$\tau = \rho_{air} \cdot C_d \cdot U_{air}^2 \quad (2.4)$$

These equations are subject to corrections based on temperature and wind speed.

2.3.4 Open Channel Flow

Chanson (2004) considers open channels as systems that flow with a free surface, with examples being streams, rivers, canals, sewers and drainage ditches. The main parameters affecting open channel flows are:

- **Geometry of the Channel:** The width, slope and roughness of the channel, which can cause the free surface to rise and fall.

- Fluid Properties: Density and viscosity.
- Flow Parameters: Velocity and flow depth.

The primary focus of open channel analysis is to find the location of the unknown free surface, by simultaneous solving the continuity and momentum equations. A simplification of the momentum equations along a streamline assuming frictionless fluid, constant gravity and incompressible flow, can be rearranged to derive the Bernoulli equation:

$$\frac{P}{\rho} + gz + \frac{\vec{V}^2}{2} = \text{constant} \quad (2.5)$$

meaning that the total sum of kinetic energy, potential energy and pressure work must remain constant. For example, as potential energy decreases: such as height of the free surface; then velocity or pressure of the fluid must increase. Open channel flow varies from pipe flow in that movement is driven by gravity rather than pressure, and the pressure at the free surface is only atmospheric.

2.3.5 Shallow Water Equations

Vallis (2019) states that the shallow water equations are used to describes a shallow layer of fluid, which is of constant density, has a free surface at the top (or bottom) and where the horizontal scale of the flow is much greater than the layer depth. Shallow water theory is complicated, and even the deepest ocean waves may be considered shallow water. Feldmeier (2019) explains that since the tidal force acts at a maximum on the surface to zero at the earths centre, the water depth is only a fraction of the radius of the Earth. Since the driving material force does almost not vary over the water column in the vertical direction, the tidal waves can be considered shallow water per se (Feldmeier 2019).

The shallow water equations are a system of hyperbolic/parabolic partial differential equations that govern fluid flow for bodies of fluid that mean the shallow water definition. They can almost always able to be applied to rivers and channels (Dawson & Mirabito 2008). They are derived from the Navier-Stokes equations and simplify the problem of a three-dimensional fluid motion to a two dimensional one, with a height-field representation. A basic version of the SWE's can be written as:

$$\frac{\partial \eta}{\partial t} + (\nabla \eta) \vec{V} = -\eta \nabla \cdot \vec{V} \quad (2.6)$$

$$\frac{\partial \vec{V}}{\partial t} + (\nabla \vec{V}) \vec{V} = a_n \nabla h \quad (2.7)$$

Where η represents the height of the fluid above the ground, \vec{V} is the velocity and a_n is the vertical acceleration of the fluid. Kayaking events are carried out on lakes and other bodies of water where the shallow water theory will likely be relevant.

2.3.6 Kelvin Ship Waves

Kelvin Ship Waves refer to the V-shaped waves left behind objects travelling on calm, deep water, as shown in figure 2.2. The wake pattern has been observed to be a wedge-shaped pattern with a half angle of 19.5° , regardless of the ships speed, as long as the deep water condition is satisfied (Fang et al. 2011). The waves created by a ship, and the energy they contain, have been of interest in hydrodynamics because of their impact on the ships motions through the drag created. In assessing the deep water condition for ships, a typical ship speed of 10m/s requires a water depth of more than 5.6m (Fang et al. 2011). The Kelvin ship wave theory will have relevance to the wave-drag acting on the kayak moving through water, as long as the deep water conditions are met.

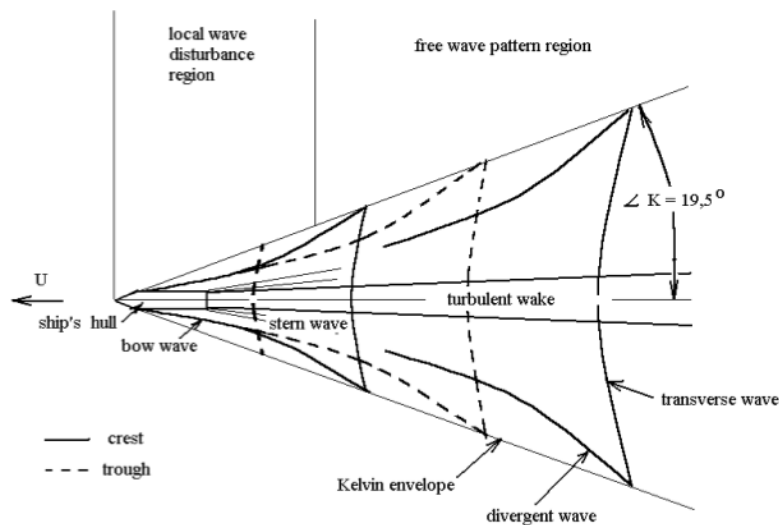


Figure 2.2: Scheme of a ship wake (Fang et al. 2011)

2.4 Drag

Pritchard & Mitchell (2015) describe drag as “the component of force on a body acting parallel to the direction of relative motion.” In the kayak system, the drag forces act in opposition to the forward motion of the kayaker created by the aft movement of the paddles in the water. This includes aerodynamic and hydrodynamic drags, above and below the waterline. Drag forces are generally divided into three categories:

- Parasitic drag
- Lift induced drag, and
- Wave drag.

The term Parasitic drag is used referring to the combination of form drag and skin friction drag, both of which are a result of an object moving through a fluid.

The drag equation is used to calculate the drag force, and is dependent on the fluid’s compressibility and density of the fluid (ρ), the velocity of the object (\vec{V}), the size and shape of the object and the viscosity of the fluid (μ) (Pritchard & Mitchell 2015). The equation is commonly displayed as:

$$F_D = \frac{1}{2}C_D\rho\vec{V}^2A \quad (2.8)$$

Within equation (2.8), C_D is the drag coefficient and A the frontal area of the object. The drag coefficient is composed of two parts, parasitic drag and the lift induced drag components, the latter used in the case of wings or other aerofoils. The drag coefficient represents the complex dependencies of shape, inclination and flow condition and is usually found experimentally from measured drag forces.

2.4.1 Pressure Drag

Pressure drag, also known as form drag or profile drag, is caused by the separation of the boundary layer from a surface and the wake created by that separation (Skybrary 2017), and is governed on the shape of the object making contact with the fluid. As the boundary layer thickens, and

particularly when boundary later separates, the pressure drag increases. The pressure drag is proportional to the difference between the pressures acting on the front and back of immersed bodies and the frontal area, as shown in figure 2.3. From this definition, the pressure drag can be simplified as the pressure difference over the area as:

$$F_{D,form} = \Delta P \cdot A \quad (2.9)$$

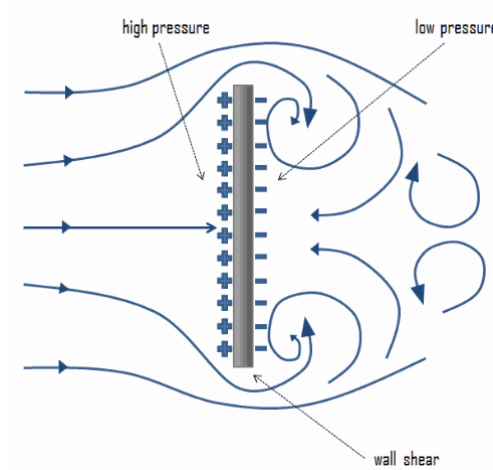


Figure 2.3: Mechanism of Pressure Drag, with flow separation aft of plate (NuclearPower 2020)

2.4.2 Friction Drag

Friction/Skin friction drag is the result of the no slip condition at the surface of the boundary layer along an object, causing shear forces due to the viscous effect of the fluid (Connor 2019). This zero-velocity fluid at the surface of an object slows down the neighbouring fluid. The region of this lower velocity fluid is referred to as the boundary layer, and the accumulation of the resistance of this region accounts for skin friction. A visual representation of a boundary layer is shown in figure 2.4, and shows the transition from laminar airflow to turbulent. Friction drag is proportional to the surface area of an object, as the further a fluid flows along an object the boundary layer thickness, and likely turbulence, increases.

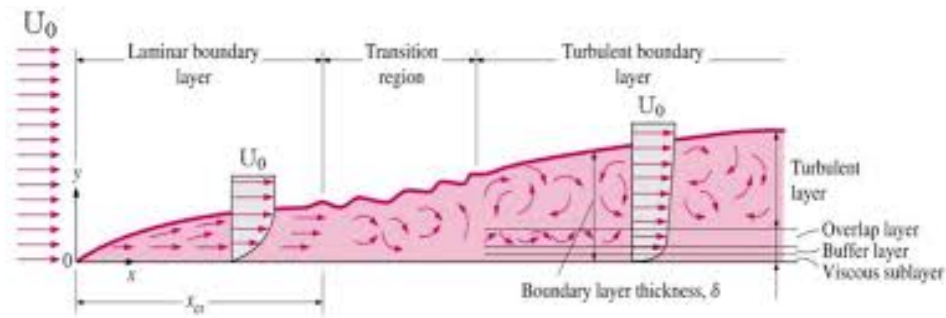


Figure 2.4: Boundary Layer of an Object, accounting for Friction Drag (NuclearPower 2020)

2.4.3 Lift-Induced Drag

Lift induced drag is a by-product of the lift force produced in aerofoils and hydrofoils, such as aircraft wings. Perfected-Flight (2020) defines induced drag on an aircraft as being caused “by the air spilling over the wingtips causing wingtip vortices, span-wise flow, increased downwash, and inefficiency.” Lift induced drag primarily affects aircraft producing large amounts of lift required for flight, however it is also a factor in watercraft that travel on the plane at high speeds. Kayak designs are long and narrow and are not prone to planing even at the fastest possible speeds.

2.4.4 Wave Drag

Wave drag can refer to either the aerodynamic wave drag on an aircraft moving at transonic or supersonic speeds, or the wave-making resistance caused by a watercraft. The wave drag on an aircraft is “due the unstable formation of shock waves which transforms a considerable part of the available propulsive energy into heat, and to the induced separation of the flow from the aircraft surfaces” (*Transonic Flow* 2020). As supersonic flow is reached, this flow stabilises and the wave drag coefficient lowers.

In the context of hydrodynamics, the waves that propagate away from a vessel carry with them energy that directly relates to the additional component of drag of a ship (Brennen 2018). The drag force is equal and opposite to the force imposed by the ship on the ocean to create the waves. This wave drag coefficient increases with the Froude number, and is dependent on the wetted area and length of the vessel.

Although the environments of aerodynamic and hydrodynamic wave drag are vastly different, it is essentially the same mechanism that leads to the increase in drag in both of these cases (Brennen 2018). In reference to kayaking, hydrodynamic wave drag will be a factor, whereas aerodynamics wave drag will not.

2.5 Dimensionless Numbers

When neither the drag force or drag coefficient is known, equations using dimensionless numbers such as the Reynolds, Bejan and Froude numbers can be implemented to assist in finding flow parameters. These numbers are important to analysis of fluid systems as they allow comparison between other systems even at different scales. The coefficients themselves can be derived from the results and compared to other literature for validation.

Different dimensionless numbers identify properties about different aspects of the kayak model. The Reynolds and Froude number describe the flow characters of the fluids. The Drag coefficient and Bejan number can help derive the drag force. The Bejan number is relatively new to fluid mechanics, and its inclusion to the review is to determine if energy or heat transfer analysis of kayak motion may be useful in the simulation or as further research.

2.5.1 Reynolds Number

One of the most important dimensionless numbers found in fluid mechanics is the Reynolds number, which is the ratio of inertial forces to viscous forces:

$$Re = \frac{\rho \vec{V} L}{\mu} \quad (2.10)$$

where L is the size scale of the flow and μ is the dynamic viscosity. Other variants of the equation substitute $\frac{\rho}{\mu}$ for $\frac{1}{\nu}$, with ν being the kinematic viscosity. Subject to context, a “large” Reynolds number indicates that viscous forces are negligible, whereas a “small” number will show that viscous effects are dominant (Pritchard & Mitchell 2015). This number is used frequently in fluid mechanics by determining whether the fluid flow can be categorised as inviscid or viscous flow; and if viscous, whether the flow is laminar or turbulent. For kayaking, the Reynolds number will be

important in calculating the type of drag forces which will be dominant, and whether flow should be modelled as laminar or turbulent.

2.5.2 Froude Number

The Froude number finds application in hydrodynamics, and can be approximated as the ratio of inertial forces to gravity forces (Pritchard & Mitchell 2015), expressed as:

$$Fr = \frac{\vec{V}}{\sqrt{gL}} \tag{2.11}$$

where g is gravity, and L is the characteristic length of the flow field, or in the case of open-channel flow, it is the water depth. Encyclopaedia Britannica (Froude number 2020) describes the applications of the Froude number as “entering into formulations of the hydraulic jump (rise in water surface elevation) that occurs under certain conditions, and together with the Reynolds number, it serves to delineate the boundary between laminar and turbulent flow conditions in open channels.” Typical Froude numbers and their effect on watercraft is shown in Figure 2.5

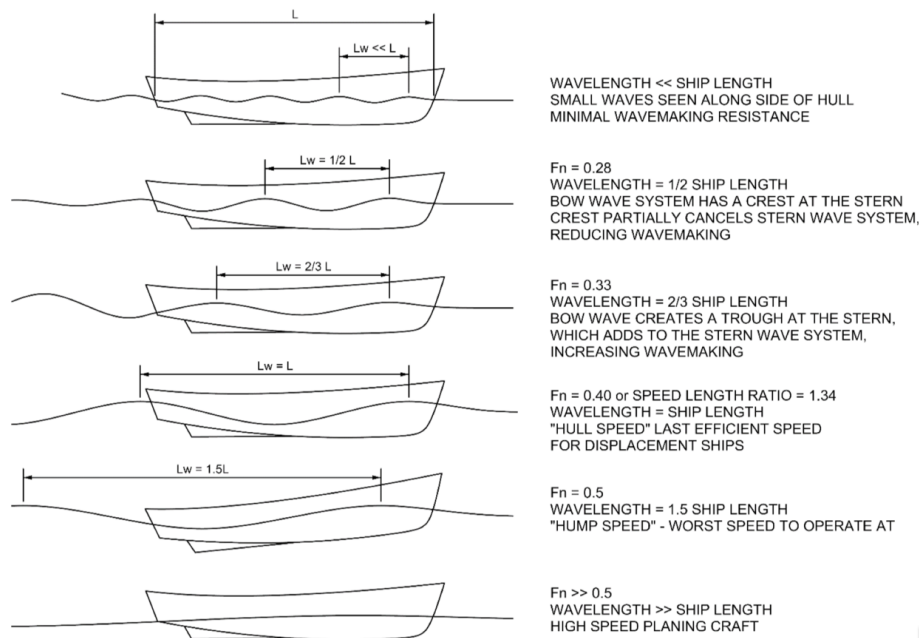


Figure 2.5: Froude number as Wave pattern Vs Speed (Vallis 2019)

2.5.3 Drag Coefficient

The drag coefficient is the dimensionless number which is a function of the complex drag parameters, such as shape, inclination and surface roughness, found at a particular Reynolds, Froude or Mach number. Due to the complex dependencies involved in calculating the drag coefficient, it is almost always found experimentally (Hall 2015a) by measuring the drag force (F_D) and deriving the drag coefficient as:

$$C_D = \frac{2F_D}{\rho \vec{V}^2 A} \quad (2.12)$$

2.5.4 Bejan Number

The Bejan number ties together aspects of fluid mechanics and heat transfer, allowing the drag coefficient to be related to the second law of thermodynamics (Trancossi & Pascoa 2018), that entropy always increases in an isolated system. There are two different Bejan Numbers, one for heat transfer and another for fluid mechanics. This section refers to the Bejan number related to fluid mechanics, where it is a dimensionless number based on the pressure drop along a contact length (L) between flow and boundaries, expressed as:

$$Be_l = \frac{\Delta P L^2}{\mu D_m} \quad (2.13)$$

where ΔP is the pressure change, μ is the dynamic viscosity and D_m is the momentum diffusivity. Trancossi & Pascoa (2018) have incorporated the Bejan number into the drag coefficient equation as:

$$C_D = 2 \left(\frac{A_w}{A_f} \right) \left(\frac{Be_l}{Re_l^2} \right) \quad (2.14)$$

Where A_w is the wetted area and A_f is the frontal area. This relationship allows the substitution of thermodynamic properties as a method of finding the drag coefficient such that:

$$C_D = \frac{2T_0 \dot{S}'_{gen}}{A_f \rho \vec{V}^3} = \frac{2\dot{X}'}{A_f \rho \vec{V}^3} \quad (2.15)$$

Where \dot{S}'_{gen} is the rate of entropy generation, \dot{X}' is the exergy dissipation rate, and T_0 is the initial

temperature. It has been researched in regards to the aeronautic sector, utilising the second law of thermodynamics as an alternate analysis of the nature of friction, instead of the more mainstream thermodynamic first law approach.

Using this coefficient relies on measuring the losses of energy within the system, typically as heat and work. It will not be relevant for the simulation, however practical field testing in the future may provide opportunities for temperature testing, and the Bejan equations may be able to assist in validation. To date, the method has been successfully used for internal fluid flow problems for incompressible fluid flow.

2.6 Computational Fluid Dynamics

Modern analysis of systems involving fluid flow, heat transfer and associated phenomena such as chemical reactions are carried out by the use of computer-based simulation known as Computational Fluid Dynamics, often abbreviated to CFD. Due to the complexities of fluid mechanic or thermodynamic problems, it is not feasible to carry out accurate hand calculations for complex fluid flows. CFD also offers a visual interface which assists in an engineer's understanding of the simulation. CFD is based around the use of the Navier-Stokes equations for analysis of the flow properties of a fluid, which are then solved by the most appropriate technique.

There are three distinct streams of numerical solution techniques: The finite difference, finite element and spectral methods. Most well established CFD codes, such as FLUENT, PHOENICS and CFX/ANSYS, utilise the finite volume method of numerical solution technique, which is an evolution of the finite difference method (Versteeg & Malalaseker 2007). The Finite Volume numerical algorithm consists of:

- Integration of the governing equations of fluid flow over all the (finite) control volumes of the domain
- Discretisation - conversion of the resulting integral equations into a system of algebraic equations
- Solution of the algebraic equations by an iterative method

There are a number of ways these steps can be achieved, based on the type of CFD model and the

required outcomes.

2.6.1 Transport Equations

The transport equations are used within fluid mechanics to describe the relationship between a fluid's velocity ($\vec{V} : (u, v, w)$), pressure (P), temperature (T) and density (ρ). They are based on the three conservation laws: conservation of mass, conservation of momentum and conservation of energy. All of Computation Fluid Dynamics is based on these equations (Anderson 2013). The full set of transport equations consist of a time-dependant continuity equation for conservation of mass (2.16), three time-dependant conservation of momentum equations (2.17-2.19) and a time-dependant conservation of energy equation (2.20) (Hall 2015*b*):

- Continuity:

$$\frac{\partial \rho}{\partial t} + \frac{\partial(\rho u)}{\partial x} + \frac{\partial(\rho v)}{\partial y} + \frac{\partial(\rho w)}{\partial z} = 0 \quad (2.16)$$

- X-Momentum:

$$\frac{\partial(\rho u)}{\partial t} + \frac{\partial(\rho u^2)}{\partial x} + \frac{\partial(\rho uv)}{\partial y} + \frac{\partial(\rho uw)}{\partial z} = -\frac{\partial P}{\partial x} + \frac{1}{Re_r} \left[\frac{\partial \tau_{xx}}{\partial x} + \frac{\partial \tau_{xy}}{\partial y} + \frac{\partial \tau_{xz}}{\partial z} \right] \quad (2.17)$$

- Y-Momentum:

$$\frac{\partial(\rho v)}{\partial t} + \frac{\partial(\rho uv)}{\partial x} + \frac{\partial(\rho v^2)}{\partial y} + \frac{\partial(\rho vw)}{\partial z} = -\frac{\partial P}{\partial y} + \frac{1}{Re_r} \left[\frac{\partial \tau_{xy}}{\partial x} + \frac{\partial \tau_{yy}}{\partial y} + \frac{\partial \tau_{yz}}{\partial z} \right] \quad (2.18)$$

- Z-Momentum:

$$\frac{\partial(\rho w)}{\partial t} + \frac{\partial(\rho uw)}{\partial x} + \frac{\partial(\rho vw)}{\partial y} + \frac{\partial(\rho w^2)}{\partial z} = -\frac{\partial P}{\partial z} + \frac{1}{Re_r} \left[\frac{\partial \tau_{xz}}{\partial x} + \frac{\partial \tau_{yz}}{\partial y} + \frac{\partial \tau_{zz}}{\partial z} \right] \quad (2.19)$$

- Energy:

$$\begin{aligned} \frac{\partial(E)}{\partial t} + \frac{\partial(uE)}{\partial x} + \frac{\partial(vE)}{\partial y} + \frac{\partial(wE)}{\partial z} &= -\frac{\partial(uP)}{\partial x} - \frac{\partial(vP)}{\partial y} - \frac{\partial(wP)}{\partial z} \\ + \frac{1}{Re} \left[\frac{\partial}{\partial x} (u\tau_{xx} + v\tau_{xy} + w\tau_{xz}) + \frac{\partial}{\partial y} (u\tau_{xy} + v\tau_{yy} + w\tau_{yz}) + \frac{\partial}{\partial z} (u\tau_{xz} + v\tau_{yz} + w\tau_{zz}) \right] \\ &\quad - \frac{1}{RePr} \left[\frac{\partial q_x}{\partial x} + \frac{\partial q_y}{\partial y} + \frac{\partial q_z}{\partial z} \right] \end{aligned} \quad (2.20)$$

Where τ is stress, t is time and q is heat flux. When simplified, the conservation laws state that: Mass is conserved; $F = mA$; and energy is conserved.

2.6.2 Navier Stokes Equations

Historically the original Navier-Stokes equations are identified as the momentum equations 2.17, 2.18 and 2.19 of the previously mentioned transport equations. This set of equations were discovered independently by 19th century mathematicians Claude-Louis Navier and George Gabriel Stokes, and were since named in their honour. Anderson (2013) explains that for modern CFD literature, the term ‘Navier Stokes Equations’ have been expanded to include the entire system of transport equations - continuity, energy and momentum. As such, most CFD literature referring to the complete Navier-Stokes equations simply means a solution using the full set of governing transport equations detailed in section 2.6.1.

For cases involving incompressible flow the energy equation cannot be included, as it decouples from the momentum and continuity equations (Henningson & Berggren 2005). In this situation the equations are referred to as the Incompressible Navier-Stokes equations. The energy equation will be required for simulations dealing with temperature changes as it is the only equation which deals with heat flux and the transfer of heat energy.

2.6.3 Meshing

ANSYS (ANSYS 2020) describes the meshing process as an integral part of the simulation process, where “complex geometries are divided into simple elements that can be used as a discrete local approximations of the larger domain”. The ANSYS user guide (ANSYS 2020) prompts users to consider set-up time, computational expense and calculation speed requirements when selecting a mesh type. The mesh shapes available within ANSYS are shown in Figure 2.6

In meshing complex geometries, Versteeg & Malalaseker (2007) offers two grid arrangement methods: Structured Curvilinear and Unstructured. Structured curvilinear, or body-fitted grids, map the flow domain with a simple shape, and are suitable for domains where the geometries are not too complex. A basic cartesian structured grid is easy to apply, however often results in wasted computational resources by having unnecessary cells within the domain. The same number of cells, applied in a body fitted grid, allows for greater computational efficiency by eliminating this waste. Figure 2.7a shows examples of Orthogonal and Non-Orthogonal body fitted meshes. Improving further on efficiency are block structured grids, which divide the domain in sub-regions each with its own structured mesh. This allows for finer meshing to be applied around objects or boundary

Common Types of Mesh

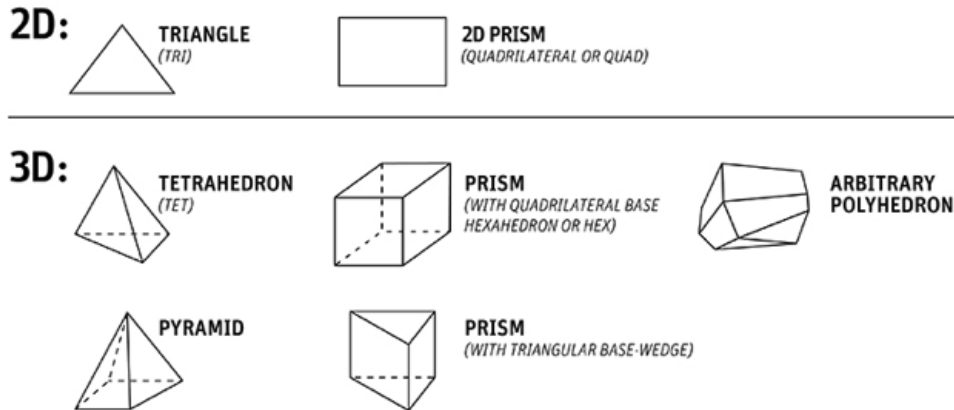
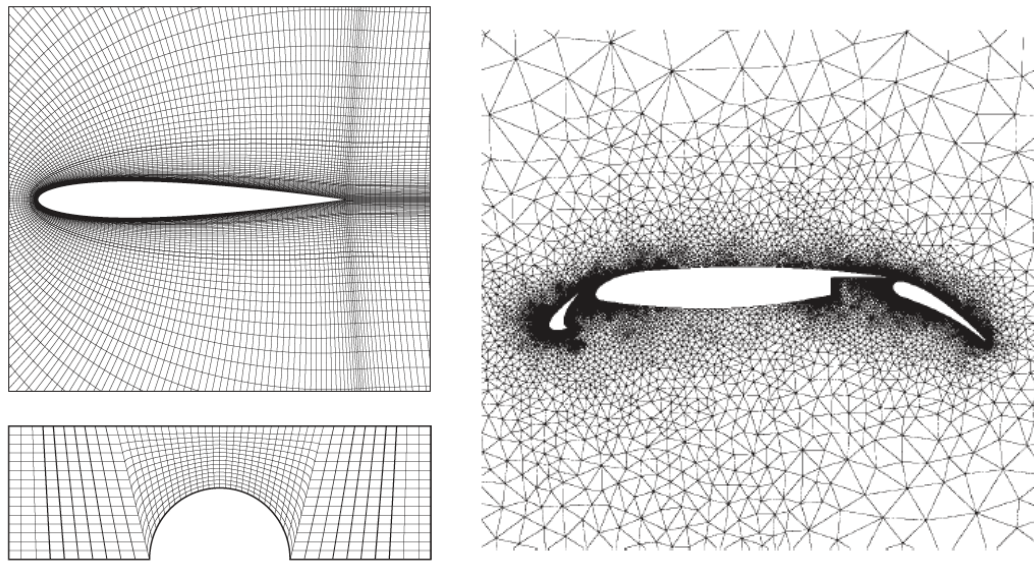


Figure 2.6: Common 2D and 3D Meshes in ANSY Fluent (ANSYS 2020)

layers, while still maintaining the ease of generation and computational simplicity of the structured method.

Unstructured grids are a step further on block structured mesh, where it can be thought of as a multi block grid where each individual cell can be treated as a block (Versteeg & Malalaseker 2007). The advantage of not being constrained by an arranged grid allows for much greater flexibility in the size and location of cells. Unstructured grids are the most efficient computationally in the case of complex flows, and are now widely used in industry and in all commercial CFD codes today (Versteeg & Malalaseker 2007). Figure 2.7b shows an unstructured mesh over a three-section aerofoil. Mesh shape is also a consideration for CFD. An article by Peric & Ferguson (2005) comparing Tetrahedral and Polyhedral meshes found that polyhedral meshing needs approximately four times fewer cells, half the memory and a tenth to fifth of the computing time to reach solutions of the same accuracy as tetrahedral meshes. The major advantage of the polyhedral method stems from the high number of sides increasing the number of neighbouring cells. This provides far greater accuracy, more than compensating for the higher storage and computing operations per cell which come with increased neighbours. From testing, Peric & Ferguson (2005) found that the result from 65513 polyhedral cells produced a more accurate result than a tetrahedral mesh of 393273 cells (approximately 6 times more).



(a) Structured Orthogonal (Top) and Non-Orthogonal (Bottom) Meshes (b) Unstructured Mesh over a three section aerofoil

Figure 2.7: Differences between Structured and Unstructured Meshes (Versteeg & Malalaseker 2007)

2.6.4 RANS Turbulence Models

Frei (2017) offers that for fluid flows containing turbulence, it becomes computationally unfeasible to resolve the small eddies, spatial and temporal scale of the oscillations with the Navier-Stokes equations. Therefore, CFD problems implement a Reynolds-Averaged Navier-Stokes (RANS) solution, which finds a time averaged sense of the problem. Frei (2017) identified seven RANS turbulence models, which can be summarised as:

- **L-VEL and yPlus:** computes the eddy viscosity using algebraic expressions based only on the local fluid velocity and distance to the closest wall. They are the most robust, least computationally intensive and generally the least accurate. They can provide good approximations for some internal flow applications. L-VEL is a combination of L (distance from the nearest wall) and VEL (the local and laminar velocity).
- **Spalart-Allmaras:** Adds a single additional variable for undamped kinematic eddy viscosity. It is relatively robust, and requires moderate resolution requirements. It is limited in accurately computing fields that exhibit shear flow, separated flow or decaying turbulence. This model was developed for the aerospace industry for the testing of aerofoils.

- **k- ϵ** : This method solves for the turbulent kinetic energy (k), and the rate of dissipation of turbulent kinetic energy (ϵ). Some advantages are that it has a good convergence rate with relatively low memory requirements. Some of its limitations are simulations including adverse pressure gradients, strong curvature or jet flows. It performs well for external flow problems around complex geometries.
- **k- ω** : is similar to the k- ϵ method however it solves for specific rate of dissipation of kinetic energy, rather than the rate of turbulence kinetic energy. It requires a good initial guess and is harder to converge than k- ϵ , however it can be useful for cases such as internal flows, strong curvature, separated flows and jets, which are typically weaknesses of the k- ϵ model.
- **Low Reynolds Number k- ϵ** : This is an extension of the standard k- ϵ method that does not require wall functions. it generally requires a denser mesh. It uses range from computing lift and drag forces, heat fluxes and separation and reattachment cases.
- **SST k- ω** : Is a combination of k- ϵ in the free stream and k- ω near the walls. The combination eliminates the some of the weaknesses displayed by the individual components, and is popular in industry. SST is an abbreviation for shear-stress transport.
- **v2-f**: This method adds two additional equations to the k- ϵ model, describing the turbulent velocity fluctuations normal to the streamlines, and a second equations accounting for non-local effects. Its purpose is to account for the fluctuations of velocity near the wall boundaries

The ANSYS user guide offers explanation of some of the other available models:

- **Reynolds Stress**: Regarded as the most elaborate type of turbulence model that FLUENT provides, it gives greater potential of accurate predictions for complex flows. It solves transport equations for the Reynolds stress together with an equation for the dissipation rate. Some examples of the best use cases include cyclone flows, high swirling flows in combustors, rotating flow passages and stress induced secondary flows in ducts.
- **Detached/Large Eddy Simulation**: In the Detached Eddy Simulation (DES) setting unsteady RANS models are employed in the boundary layer while the Large Eddy Simulation (LES) treatment is applied to the separated regions. It is often referred to as the hybrid LES/RANS method. DES models are useful for high Reynolds number wall bounded flows, where the cost of solving wall functions as LES would be prohibitive. The computational

costs of DES are larger than RANS yet less than LES. Within DES three different models are offered; the Spalart-Allmaras, $k-\epsilon$ and $k-\omega$.

2.6.5 Multiphase Models

Multiphase flow refers to the simultaneous presence of different phases, where phase refers to solid, liquid or vapour state of matter (Stenmark 2013). In characterising multi-phase models, the system should first be characterised. ANSYS splits them into 3 major categories; fluid-fluid flows, gas-solid flows, and liquids-solid flows. Stenmark (2013) further characterises flows according to visual appearance as separated, mixed or dispersed. The correct recognition and categorisation of these flow patterns is comparable to the importance of knowing whether a flow is laminar or turbulent in single-phase flow (Stenmark 2013).

ANSYS (ANSYS 2020) currently offers a number of options for modelling a Multiphase simulation of Gas-Liquid or Liquid-Liquid flows. The available models for a Eulerian frame of reference:

- **Volume of Fluid (VOF):** predicts the interface shape between immiscible fluid phases. Suitable for immiscible fluids separated by a clearly defined interface.
- **Algebraic Interfacial Area Density (AIAD) Model:** For flows that may include a transition between continuous stratified flows and dispersed flow regimes. Best used for mixed or transitional flows or separated flows.
- **Eulerian Model:** accurately models multiple separate, yet interacting, phases of solids, liquids or gases in any combination.
- **Mixture Model:** a simplified Eulerian model when the relaxation time of the dispersed time is small.
- **Euler-Granular:** uses eulerian approach to model dispersed particles in a continuous fluid.
- **Population Balance Model:** used for systems where particle size distributions change, such as droplet break up, nucleation or agglomeration. Typical used in combination with other models to account for particle distributions.
- **Volume of Fluid (VOF) to Discrete Phase Model (DPM):** the hybrid combination of two models, in which the VOF method tracks the interface instabilities and surface tension

effects and the DPM methods takes over to track the droplets. The VOF used the Eulerian frame of reference, whereas the DPM used the more computational efficient Lagrangian framework. Best applied to mixed or transitional flows. Further detail on DPM modelling is found in the next section.

The available models which use the Lagrangian frame of reference, suitable for dispersed flows, are:

- **Discrete Phase Model (DPM):** particle interactions are neglected. Is used for simulations where the dispersed second phase is <10%.
- **Dense Discrete Phase Model (DDPM):** An extension of the DPM model for higher volume fractions of the dispersed phase, still <30%.
- **Discrete Element Method:** Used for flows with high volume fractions, where particle-particle interaction is importance. The particle interaction with the fluid flow does not need to be a focus of this method.

The modelling of a kayak system is a fluid-fluid flow containing water and air as fluids, and the interface between them is further defined in the stratified/free surface category. Stratified/free surface interaction is applicable when "the less-dense fluid is separated from (and above) the more-dense fluid, so that each fluid forms a layer" (Wandel 2020). For this type of problem, Wandel (2020) recommends the Volume of Fluid method, and this is the selection for this project.

2.6.6 Volume of Fluid Method

The volume of fluid method (VOF) is capable of modelling two or more immiscible fluid, by solving a single set of momentum equations and tracking the volume fractions of each fluid throughout the domain (Mantha et al. 2013). The equations for a fluid would appear as:

$$\frac{1}{\rho_q} \left[\frac{\partial}{\partial t} (\alpha_q \rho_q) + \nabla \cdot (\alpha_q \rho_q \vec{V}_q) = \sum_{p=1}^n (\dot{m}_{pq} - \dot{m}_{qp}) \right] \quad (2.21)$$

where α is the volume fraction of a cell between 0 and 1, with 1 corresponding to 100% of the cell occupied by that fluid. For the mass flow rates, \dot{m}_{pq} is the mass transfer from phase p to q and \dot{m}_{qp} is the transfer from phase q to p (Mantha et al. 2013)

2.6.7 CFD Solvers

ANSYS Fluent used two solver technologies, pressure-based and density-based. Pressure-based traditionally has been used for incompressible and mildly compressible flows, while density-based was originally designed for high speed compressible flows, however both methods are now applicable for a broad range of flows (ANSYS 2013). In relation to the kayak simulation, the low air flow speed can be considered incompressible. The model selected in Section 2.6.5 was the VOF multiphase model, and research was carried out in regards to best options for this choice. The density based solver is not compatible with the multiphase model options, making it not suitable for the kayak simulation.

2.7 Chapter Summary

The literature review identified the mechanisms of drag acting on the kayaker, and provided options to simulate this as a CFD model. Pressure, friction and wave making drag all contribute to the slowing of the kayaker. The combination of water and air within the simulation also complicates the analysis, as aerodynamic and hydrodynamic understanding is required. Investigation of the best suited CFD methods identified that a Volume of Fluid model combined with an Open Channel Flow sub-model most closely represents the kayaking system. In suggesting methods for competitive advantage, pacing strategy shows the most potential, due to strict rules on boat and equipment design.

Chapter 3

Methodology

3.1 Chapter Overview

This chapter details the steps taken to create the simulation of the Kayaker meeting air and water resistance. ANSYS Fluent was selected to build the model, as it is the CFD package used at University of Southern Queensland, and features a home academic version. In building to the final model, a number of preliminary models were designed and tested to demonstrate the methods and prove the viability of ANSYS Fluent to achieve the project aims. They also allowed slight changes to be tested on individual sections or geometries, to help predict the effect the change will have on the full system.

The final methodology details the creation of the project simulation, aimed at achieving the goals set forth in Section 1.3. Decision on the methodology were made after reviewing the literature for the best way to model the kayaker and the ANSYS user guide for technical details.

3.2 FLUENT Workspace

ANSYS Fluent simulations involve creating and analysing a system in five steps: Geometry, Mesh, Setup, Solution and Results. Geometry, meshing and setup help create the system while solution and results are used to analyse the simulation. The Workbench workspace schematic is shown in Figure 3.1. A brief summary of each of the groups, and their purpose to this project are:

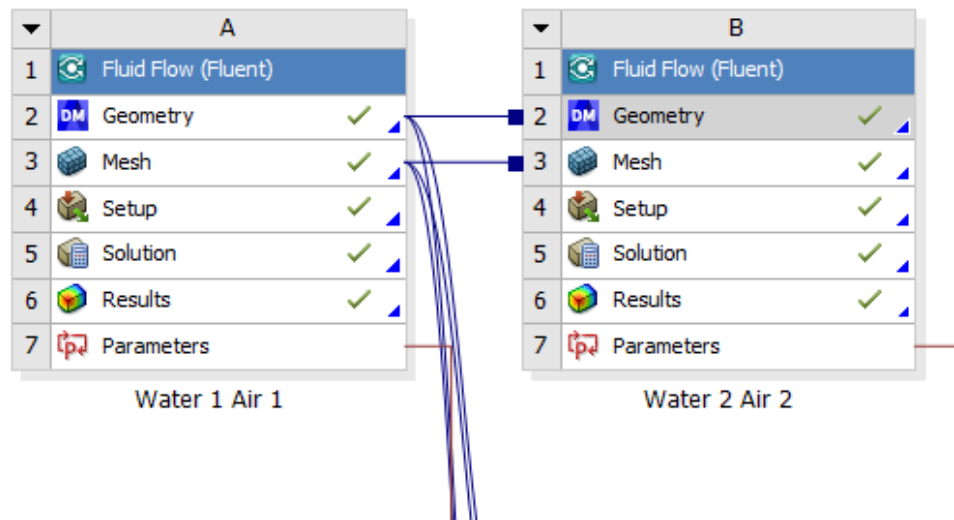


Figure 3.1: ANSYS Workbench Schematic

- **Geometry:** Used for creating or importing the simulations geometry and domain. The created geometries can be 2D representations or extruded in 3D shapes. CAD models created in other solid modelling software can be imported. Geometry do not have be solid areas of the model, and may be used a body of influence for meshing.
- **Meshing:** The meshing menu allows for the creation of any number of different sizes meshes over an object. The meshing process can be time consuming, and if areas of high activity are not meshed correctly the simulation will not provide accurate results. Too fine a mesh may result in unacceptable processing times or interference errors. One of the important activities carried out during meshing is to create named selections for any items of interest for the simulation. These can include inlets, outlets or shapes requiring analysis in the results. The named selections can be faces or volumes.
- **Setup:** The setup menu allows for customisation of all the boundary conditions and the initial state of the model. The simulation model, and turbulence model are selected here. The range of options within the setup is vast, and many of the setting are not required for this simulation. FLUENT allows for analysis of fluids, gases and heat transfer.
- **Solution:** This menu allows for re-solving of a simulation or analysis of the simulation's outputs. The convergence figures, iterations and time steps can be adjusted to suit a new required solution.
- **Results:** The results menu allows of visual and numerical analysis of the solution. A vast

array of graphics and be superimposed on the geometry to show fluid properties. The results for this project are used to show the changes in air and water flow, identifying drag.

3.3 Preliminary Simulations

After reviewing the literature, a number of preliminary simulations were required to establish the feasibility of using ANSYS FLUENT for the project. The ability to model basic shapes and determine drag force, as well as establish variable wind and water speeds were key to achieving the goals set forth in Section 1.1.1. Included in this section are the models, their intentions and preliminary results.

3.3.1 Basic Wind Simulation

The first simulation created was used for familiarity of the ANSYS software and to establish a variable wind through a control volume. A domain was created in geometry, and a course mesh created throughout the domain. An inlet and an outlet were created by the named selection command in the meshing menu. Figure 3.2 shows the course mesh, and inlet and outlet. Not shown in figure 3.2 are the other walls of the domain, which when visible created a cube domain. The

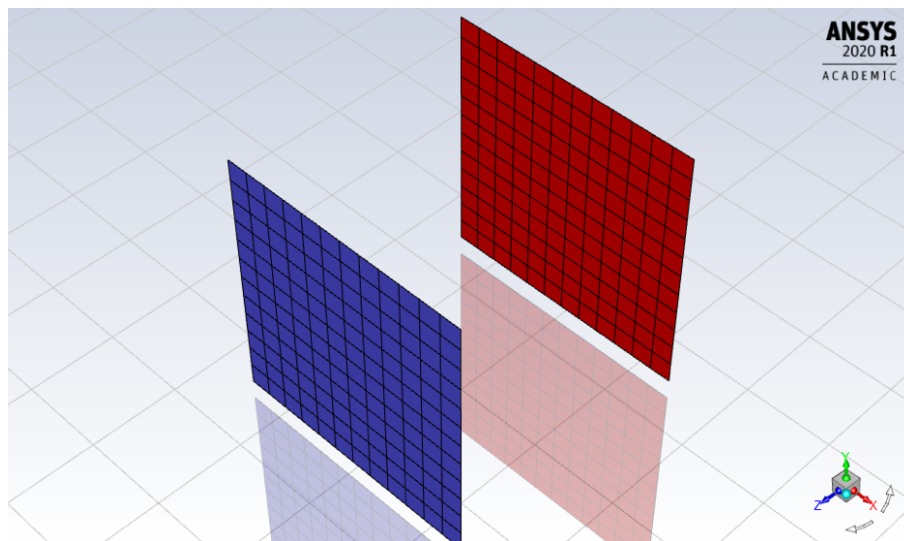


Figure 3.2: Basic Model of Wind through a domain, with Inlet (blue) and Outlet (red)

basic wind simulation provided a good visual representation of the direction and velocity changes within the wind. Although it was expected that a domain boundary layer would be present, it was

unexpected the size of the region of lower velocity air, caused by the no slip condition at the walls. For the final simulation, the domain size would need to be adequate enough to not affect the flow of fluid around the kayak or kayaker.

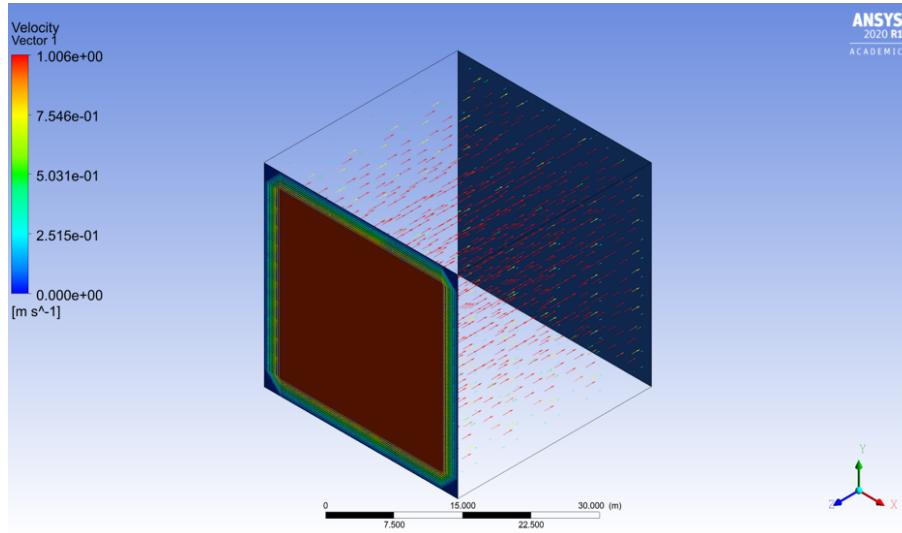


Figure 3.3: Basic Model of Wind through a domain, with Inlet (forward) and Outlet (aft)

3.3.2 Wind around Cylinder Simulation

The next simulation built upon the basic wind simulation by adding a cylinder in the centre, for the purpose of determining fluid flow around an object. After creating a new sketch and extrude, the shape was removed from the wind path via the Boolean command in ANSYS. This creates a different path for the air, as it now has to flow around the cylinder. Figure 3.4 shows the location of the cylinder, positioned in the middle of the domain.

The wind around the cylinder simulation at first did not register the cylinder, with the air continuing through the cylinder as if it didn't exist. To make the cylinder appear as a solid in the simulation, a Boolean needed to be created. The simulation was reattempted with the cylinder removed from the domain, and the results shown in Figure 3.5. The figure shows vectors applied to the streamline showing the path of the air and the changes in velocity as it diverts around the cylinder. The streamlines alone were too cluttered and did not screenshot well for the report. Further analysis found that the size of the domain was too small, not allowing the fluid stream to return to a steady state condition.

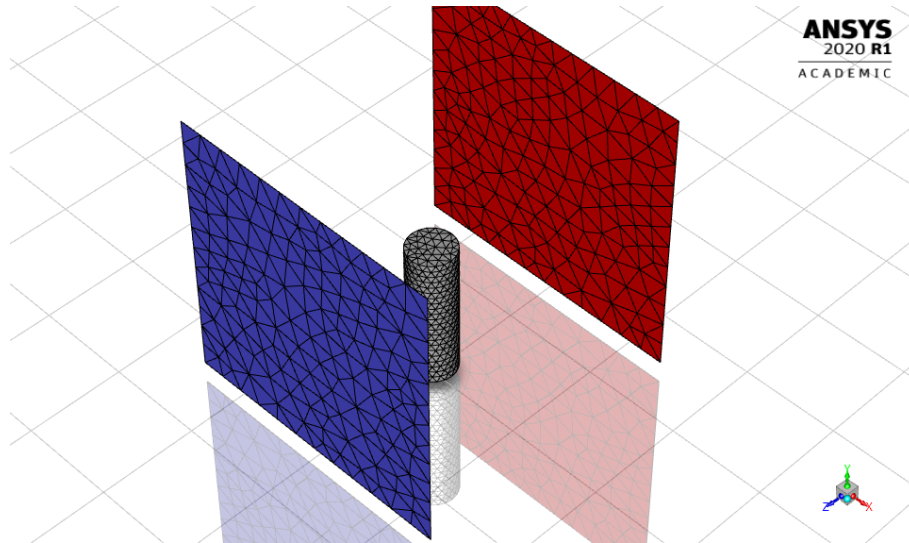


Figure 3.4: Model of Wind around a Cylinder, with inlet (blue) and outlet (red)

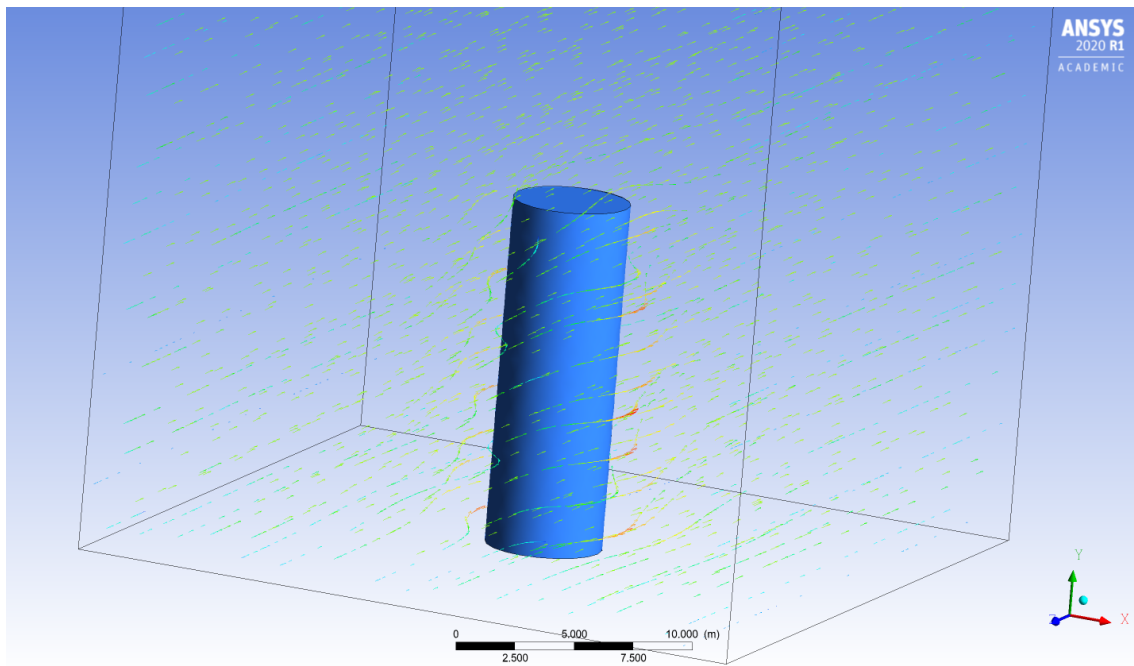


Figure 3.5: Model of Air Flow around a Cylinder showing changes in velocity

3.3.3 Kayak with Single Boundary Inlet Simulation

The Wind/Kayak system includes the option to vary the speed of the water separate to the speed of the wind. This would simulate a kayaker moving at a set velocity through the water while encountering wind at a different magnitude or direction. The resultant vector of wind applied to the model, accounting for the forward motion of the kayaker, is calculated manually before being entered into the boundary condition. The kayak motion is simulated by moving the water and air

around a stationary kayak geometry. This is was first multiphase simulation attempted, and as such was a greater level of complexity. A review of the literature found that a Volume of Fluid model was best used for this particular problem containing separated multiphase flow.

This modelled a rudimentary kayak shape travelling in water. This design was selected to compare the results to determine if the drag figures calculated matched previous research findings.

- **Geometry:** The kayak geometry created approximately matches the dimensions given by (Mantha et al. 2013) for the Nelo Vanquish, although details or refinements were not made to the shape at this early stage. An extra volume region was added to allow for a finer mesh around the kayak and expected waterline.
- **Meshing:** The kayak / waterline region was given a maximum element size of 5cm, as this is the area of importance in determining the drag force present. By only creating a finer mesh in this area, computational power and time is saved by allowing a courser mesh in areas which don't affect the calculations.
- **Setup:** The k- ϵ model was selected due to its good performance in external flow cases. An inlet air velocity of 10m/s was set as normal to the boundary. The calculation was set at 500 iterations with a time scale factor of 0.5.
- **Results:** The single boundary kayak simulation created a good result, with large regions of changing velocity present around the kayak, indicting its effect on the water. The isosurface was taken at the surface of the water, with vectors applied to streamline at this location. It was expected that the surface of the water would be flat, and it is still not known what exactly has caused the bumpy surface. It is possible that the walls of the simulation are having a larger effect on the flow than predicted. A much large enclosure may be required to ensure the walls do not cause the water to be disturbed, as only the wind and the travel of the kayak are expected to be of importance, and not the sides of the domain area.

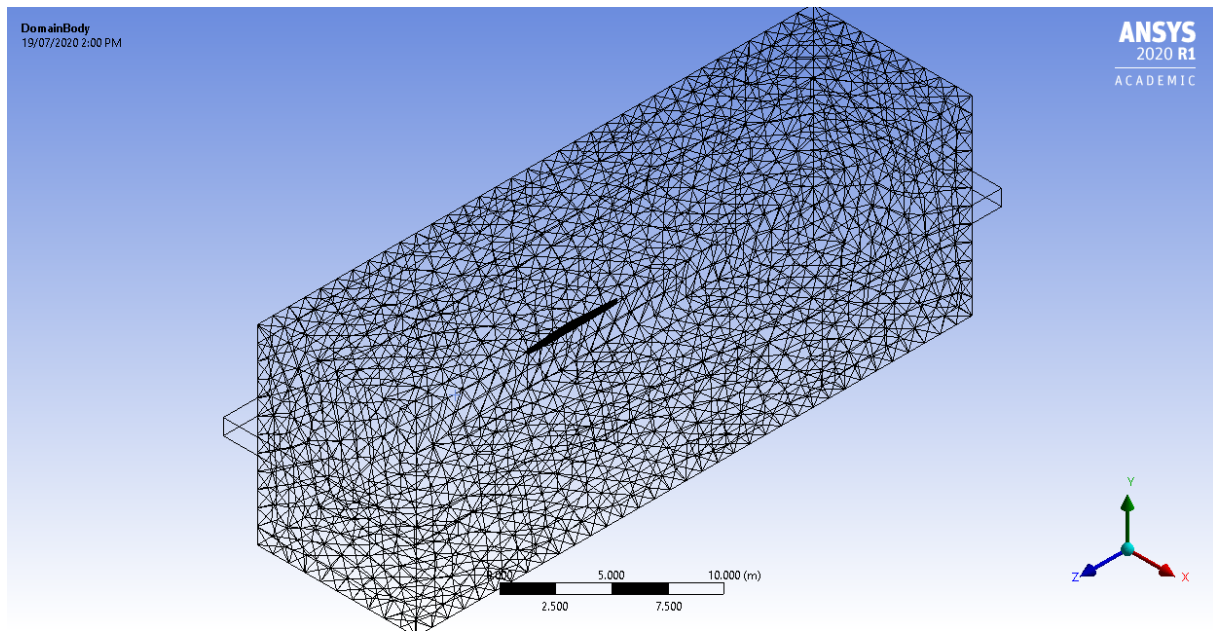


Figure 3.6: Multifluid Model of Kayak with volume region wireframe shown centrally

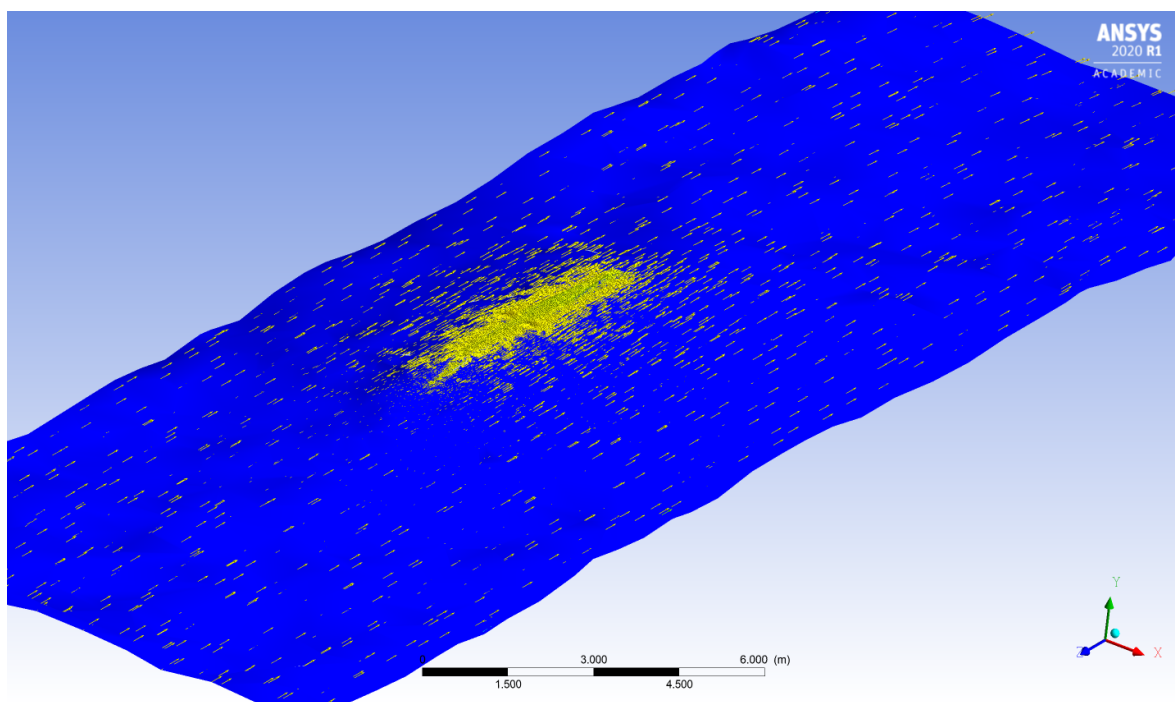


Figure 3.7: Water Velocity around a Kayak Moving through Water

3.4 Project Simulation

The final simulations created were built on the principals of the previous models to achieve the project goals set forth in Section 1.3. This is the main simulation of the project, and includes variable wind and water speeds. Drag outputs are collated and analysed for this section of the dissertation.

3.4.1 Scope

The project aim involves determining the effect of the wind on the kayaker, and this was determined by including a range of winds in the simulations which would realistically be found during competition kayaking event. The literature review found that the wind affects competitive kayaking in two ways; Increased drag on the above water portion of the kayaker, and small waves on the water's surface. Water surface waves are a function of a number of variables, such as the sides and bottom of the body of water and current flow. A large range of simulations have been created to determine the effects of both of these. Only head winds were considered, as the component of drag affecting the kayaker is only opposite to the direction of motion. Crosswind effects on the rotation of the kayaker were not considered in the scope of this dissertation.

The minimum air speed was set to equal to the water speed, as even on a still day the kayaker will still be making contact with the air at the same speed as the kayak is travelling. The maximum kayak speeds considered were 7m/s, as the record time for a 500m sprint was an average of 6m/s. The inclusion of 7m/s was required as the pacing strategy for kayakers includes an all-out start before a transition to an even pacing strategy. The maximum headwind speed considered was 10m/s, which is equivalent to 36km/h. The 10m/s was added to the static air speed, so that the inlet air boundary condition included the kayaker speed plus the headwind speed. For example, a 6m/s kayaker with a 10m/s headwind required a 16m/s inlet air velocity.

The simulations created to show the wind effects were as follows:

- Equal Water and Headwind speed: This simulation recreates a still day with no wind, which the water and air hitting the kayaker at the velocity of travel. This is carried out for speeds from 1m/s to 7m/s.

- Constant Water Speed and increasing Headwind speed: This simulates a headwind for a kayaker travelling at a set speed with a headwind relative to their forward motion. The water speeds were set from 1-7m/s, and the relative headwind from 2-10m/s.
- Constant Water Speed with small waves: This simulates a headwind creating small waves on the water's surface. This is carried out for water speeds from 4-7m. The wave size selected was 5cm in height, separated by 20 centimetres per wave, similar to small waves observed on a windy day on a river. No headwind was included for these simulations.

3.4.2 Geometry

The Kayak and athlete model created is based around dimensions for the Nelo Vanquish series Kayaks and the torso, head and upper arms of an average person. The Vanquish dimensions were based on the measurements of Mantha et al. (2013) with a 5.2m overall length and 40mm width around the centre. The geometries are kept basic, as the simulation has been created to provide analysis for a form of a kayaker and not a particular kayak or person. The waterline was set at 0.16m from the bottom of the kayak, which reflects research carried out by (Barros 2015) for hull displacement on the Nelo Vanquish during tow testing. Some other inclusions are a slightly higher above waterline portion of the kayak, added to more realistically clear the waterline, and a curved bottom. The inclusion of further detail, such as forearms and paddle, were restricted in the meshing limitations of the ANSYS academic version. The kayak geometry created is shown in Figure 3.8.

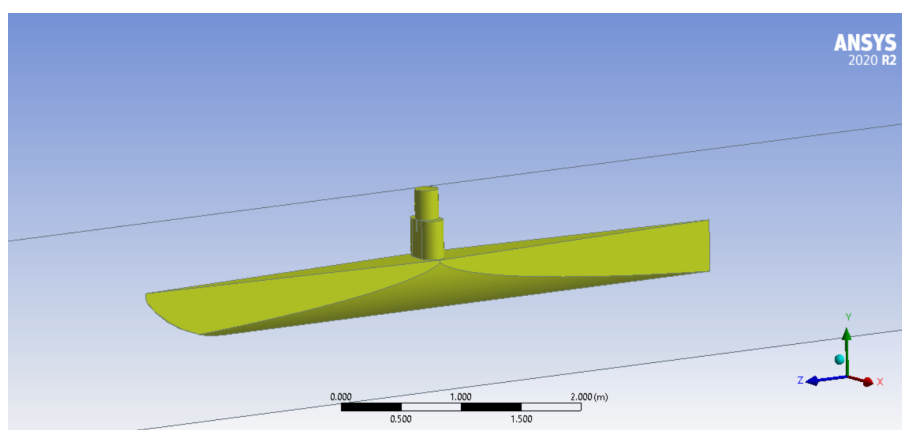
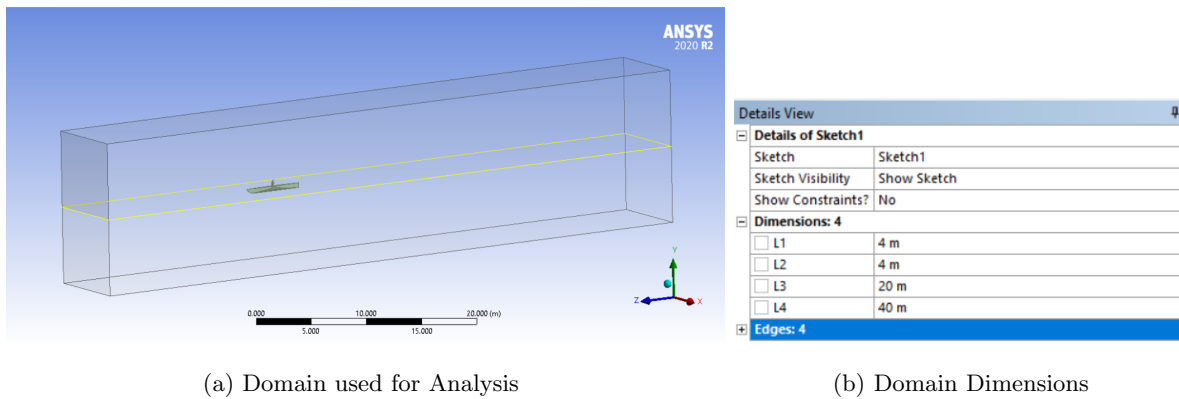


Figure 3.8: Geometry representing Kayaker

One of the initial steps within CFD is to setup a domain. Singh et al. (2017) explain that the

minimum domain size should be at least $1.3L$ forward and to each side and $5L$ aft of a hull when setting a domain for marine CFD applications. Other research for external flow domains recommends using $5-10L$ upstream and $10-20L$ downstream, where L is chord length for aerodynamics analysis (Autodesk 2020). The domain size created is conservative, adding to these minimums, with the final dimensions being 20m forward, 40m aft, and 4m either side, all measurements taken from the origin at the centre of the kayaker. The domain and dimensions are shown in Figure 3.9.

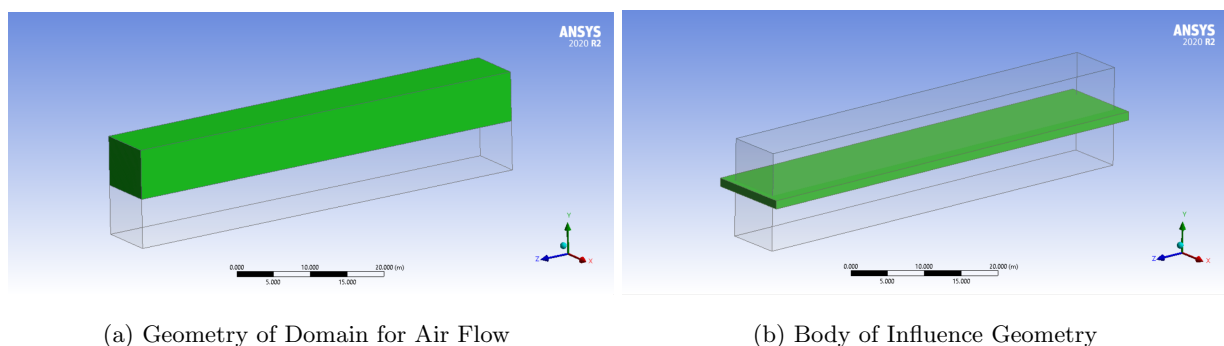


(a) Domain used for Analysis

(b) Domain Dimensions

Figure 3.9: Geometry of Project Domain

Additional inclusions made in geometry were the air body used as the secondary domain for the independent air flow, and a tertiary volume later used as a body of influence for meshing refinement, shown in Figure 3.10. A Boolean was created to remove the kayak and athlete extrusions from the domain. This ensures the path of the water and air are diverted by these shapes, and is essential for analysis. Finally, a symmetry plane was made on the YZ axis, effectively halving the geometry of the model. This was done for computational efficiency and meshing resources purposes.



(a) Geometry of Domain for Air Flow

(b) Body of Influence Geometry

Figure 3.10: Other Geometry Features

3.4.3 Meshing

The meshing selected is based around applying a fine mesh around the kayaker and waterline, and a course mesh for the free stream flow paths. This was carried out by creating a fine face mesh around the kayaker and inflating the element size out gradually. The refined mesh around the waterline was created using the body of influence option with the body meshing option. This create a volume with a custom mesh, with the body of influence visible in Figure 3.11. The result is an unstructured inflation mesh with a maximum element size at the body of influence of .2m, increasing to a global maximum set at 1.5961m. The growth rate is 1.75, therefore the maximum element sizes at the extremities of the domain decrease by a factor of 1.75 in each layer.

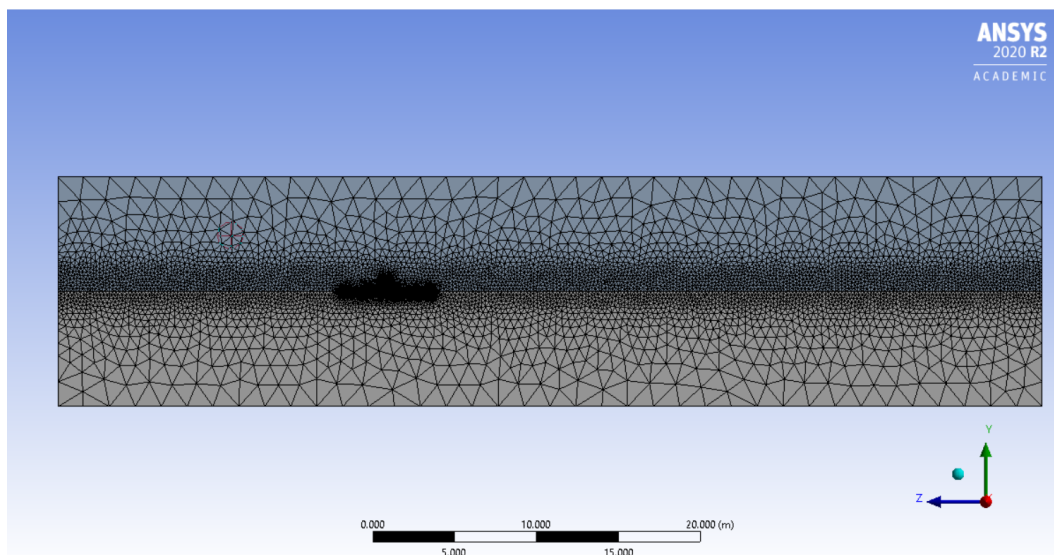


Figure 3.11: Wide View of the Mesh

The mesh size was severely restricted by the academic version only allowing a maximum element count of 512,000. This did however force the meshing to be efficient, and only applied to areas of interest. The free air stream not affected by the kayak shape was left with a very course mesh, and the finest mesh applied to the kayaker and surrounding close area. The symmetry plane created on the YZ plane effectively doubled the mesh elements available to use. The review of the literature found that polyhedral meshes are far more efficient than tetrahedral meshes, as much as a factor of 6. The mesh was therefore converted to Polyhedra in the setup menu, after initially being created as tetrahedral in the meshing menu. The body of influence uses the geometry around the waterline to improve the create a smaller mesh with the area expected for waves, as well as the flow path for air flowing over the torso and head. The created mesh around the kayak is shown in Figure 3.12.

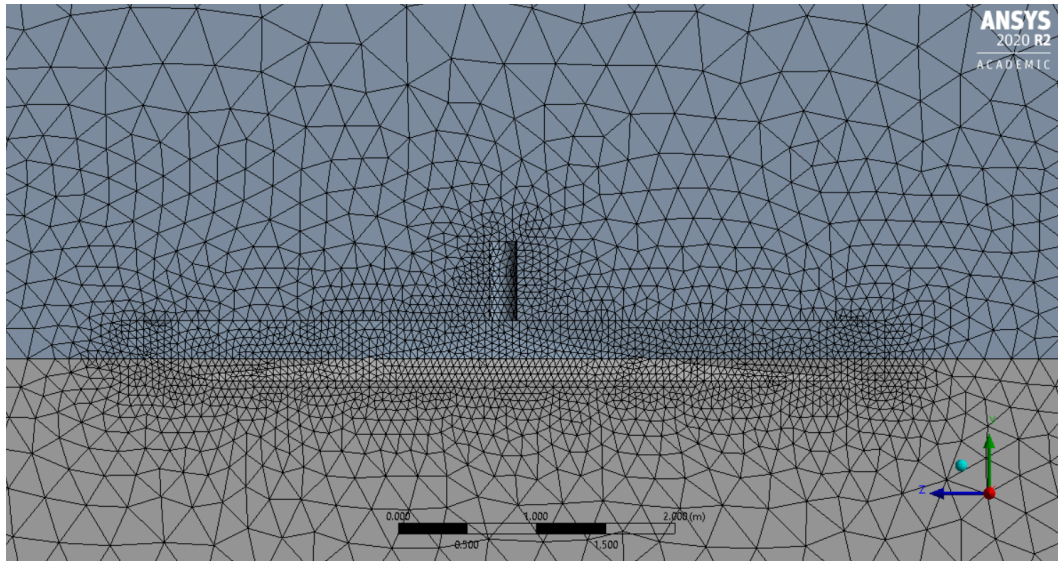


Figure 3.12: Close View of the Mesh around the kayaker

The Meshing phase is also when named selections are applied to parts of the model required for set up or analysis. The named selections created were:

- **WaterInlet:** The inlet for the water for the open channel flow boundary condition. The water inlet stretches the entire height of the domain.
- **WaterOutlet:** The outlet for the open channel flow, covers the entire height of the domain
- **AirInlet:** The air inlet is used for the variable head windspeed, and extends from the waterline (0) to the top of the domain (7m).
- **AirOutlet:** The outlet for the air flow above the waterline, from 0 to 7m in height.
- **Symmetry:** This named selection was created for post processing purposes, to enable the centre plane to be displayed showing all geometries of the model
- **Kayak:** The Kayak named selection included the all the faces of hull of the kayak and the kayaker. This is important as the total drag force is found from this area.

Figure 3.13 shows the element arrangement after conversion to a Polyhedral mesh.

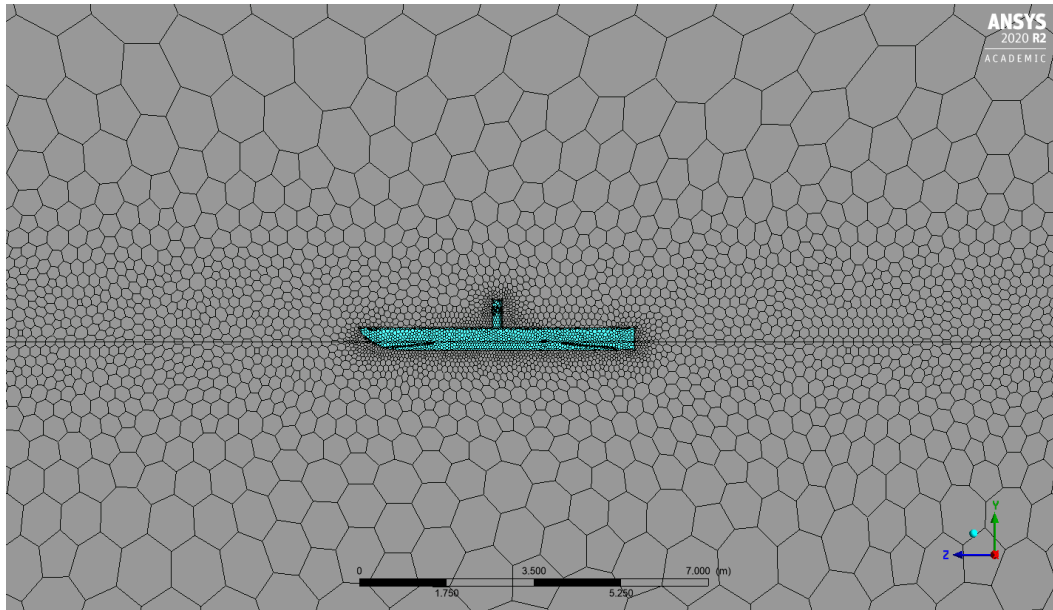


Figure 3.13: Model after conversion to Polyhedral Mesh

3.4.4 Model Selection

The model selected was the Volume of Fluid multiphase model, with water and air being the two phases. Figure 3.14 shows contours of the starting volume fractions of water for the model, with red indicating a volume fraction of 1 (100%) and blue indicating no water. For this to work, gravity was set at $-9.81m/s^2$ in the Y direction. The Transient time option was selected, to enable drag calculations for period of waves, and to get a clearer picture of the simulations and the effects of the wind on water.

Surface tension of the water/air interface was set to $.072N/m$, with the intension of producing slight waves from this interaction. The ANSYS user manual (ANSYS 2013) provides guidance on setting up the VOF model within Fluent. Inputs required are the number of phases and whether the scheme is Explicit or Implicit. Within examples, ANSYS recommended used the implicit interpolation scheme for flow around a ship's hull, which mirrors the goals of this project.

Optional choices within the multiphase model include the sub-model option for open channel flow. The literature review found that the bodies of water that host kayaking events are almost always representative of open channel flows. Selections within the open channel flow sub-model require setting the inlet as a pressure inlet, and setting open channel boundary conditions. From the literature and consultation with the ANSYS user manual, the VOF model with Open-Channel flow sub model was selected, and open channel boundary conditions applied.

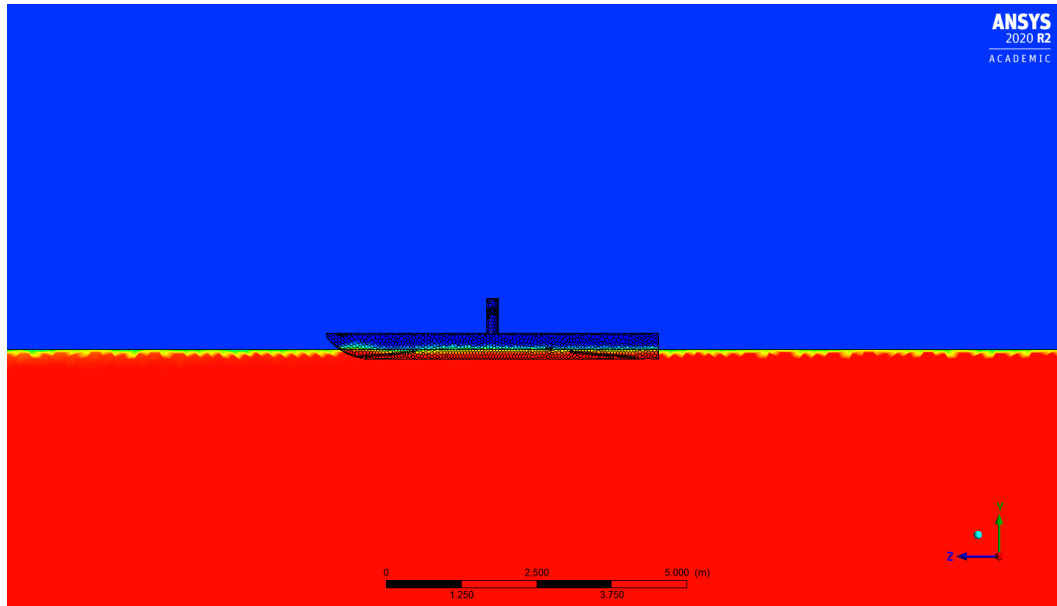


Figure 3.14: Volume Fraction of water after initialisation, red indicating water.

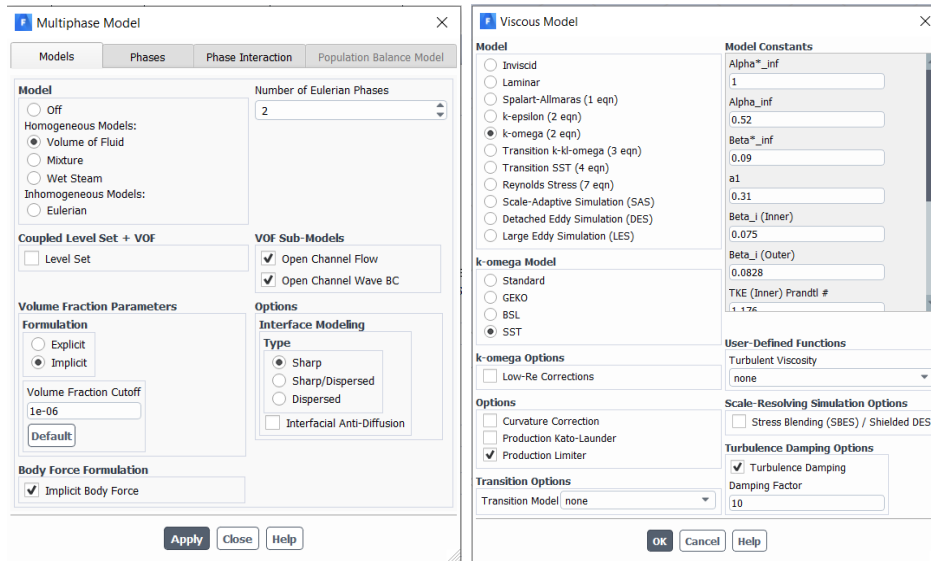
3.4.5 Turbulence Model

A number of turbulence models would be suitable for this model, however the most suitable selected was the SST $k-\omega$ model, which combines the advantages of the $k-\epsilon$ and $k-\omega$, was selected. SST $k-\omega$ applies $k-\epsilon$ in the free stream and $k-\omega$ near the walls, allowing for a coarser mesh and a greater allowable y^+ value. Borges et al. (2013) found the SST $k-\omega$ model accurate at high Froude numbers during a similar open channel hydrodynamics project.

Turbulence damping is an option within the SST $k-\omega$ model, which is required for accurate modelling of the interfacial area (ANSYS 2013) where the liquid-liquid contact occurs. This setting was left at the default of 10.

3.4.6 Boundary Conditions

The Volume of Fluid model with Open Channel sub model activated allow for the inlet and outlet boundary conditions to be changed. This requires the use of either the Pressure Inlet or Mass flow rate inlet conditions.



(a) Volume of Fluid Settings

(b) Turbulence model Selections Menu

Figure 3.15: Fluent Menu Settings

3.4.7 Solver Settings

The pressure based solver was selected, as this is mandatory in conjunction with the Volume of Fluid multiphase model. For the pressure-based solver, the user guide outlines the general procedures and considerations when setting up the solver within Fluent (ANSYS 2013):

1. **Select the pressure-velocity coupling method:** ANSYS offers four different options; SIMPLE, SIMPLEC, PISO and Fractional Step Method (FSM). SIMPLE and SIMPLEC are generally used for steady state simulations and PISO recommended for transient simulations. FSM is an option when using the Non-iterative Time advancement model. The PISO selection was made as the simulations are transient based, due to the inclusion of waves in the boundary conditions for some simulations.
2. **Choose the spatial discretization and pressure interpolation schemes:** The options for spatial discretization are Green-Gauss Cell Based, Green-Gauss Node Based, or Least Squares Cell Based. The least squares cell based is known to be as accurate as the node based gradient for irregular unstructured meshes but less expensive to compute, and is recommended. For the pressure interpolations selections, only the PRESTO! or body-weighted forces (BWF) are selectable for the VOF method. BWF is recommended for problems with large body forces, and PRESTO! for high swirl, high-Rayleigh or high rotating flows. The

Least Squares Cell Based spatial discretization and PRESTO! pressure interpolation schemes were selected, based on the ANSYS recommendations and low expected body forces.

3. **Select the porous media velocity:** Allows selection of different methods for models which include porous media such as filters or perforated plates. Not considered for the Kayak simulation.
4. **Select the method the derivatives are to be evaluated by choosing gradient options:** Each option with the Volume of Fluid method may be adjusted. When deciding between First-Order vs. Second-Order discretization options ANSYS recommends only using first-order upwind for flows which are aligned with the mesh. For triangular or tetrahedral meshes, this is never the case, and the second-order option is more accurate.
5. **Set the under-relaxation factors:** The default under relaxation factors set in ANSYS are near optimal for the largest possible amount of iterations. It is good practice to use the default number, and adjust if the residuals continue to increase after the first 4 or 5 iterations.
6. **Make any additional modifications to the solver settings that are suggested in the chapters or sections that describe the model you are using:** The Volume of Fluid model, or open channel flow guide do not make any special recommendations for these settings.
7. **Enable the appropriate solution monitors:** The convergence criteria figures were set at $1e^{-4}$ for continuity, x-y-z velocities, k, omega and vf-phase 2. The default setting was $1e^{-3}$, however this represents rather low accuracy. The convergence criteria selected met a good balance of accuracy and computational time. The drag calculations required did not need to be highly accurate, merely representative of the drag increases with wind speed.

Two reports were created, monitoring drag within the waterbody, and airbody domains. The outputs for the drag calculations are set to a parameter set, which collates all the drag figures and the simulation it originates from. The drag calculations are also graphed and shown on an output during solving.
8. **Initialise the solutions:** Before initialisation, a volume region was created on the bottom half of the waterbody. This is the section of the domain which starts the simulation filled with water, and must be patched within the initialisation menu. The 'Open Channel Initialisation Method' is set to Flat for simulations that don't feature waves, and wavy for those that do.

9. **Start calculating:** All simulations were set for time steps of 0.1s for 100 time steps, equally a total of 10sec. The iterations were initially set to 100 per time step, with the option to adjust if convergence criteria were not met.
10. **If difficulty in converging, consult user guide for methods:** The final step of using the solver is to run the simulation and observe the residuals, drag outputs and volume fractions to ensure the simulation is running smoothly. If errors are noticed, it is more efficient to stop the calculation and rectify immediately.

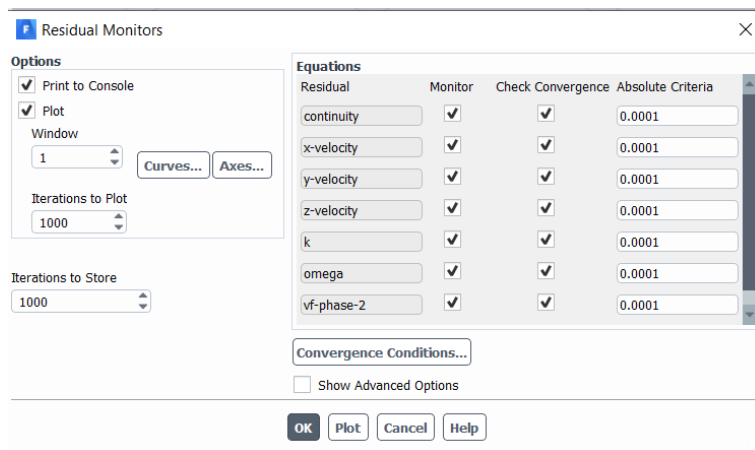


Figure 3.16: Convergence settings for the simulation

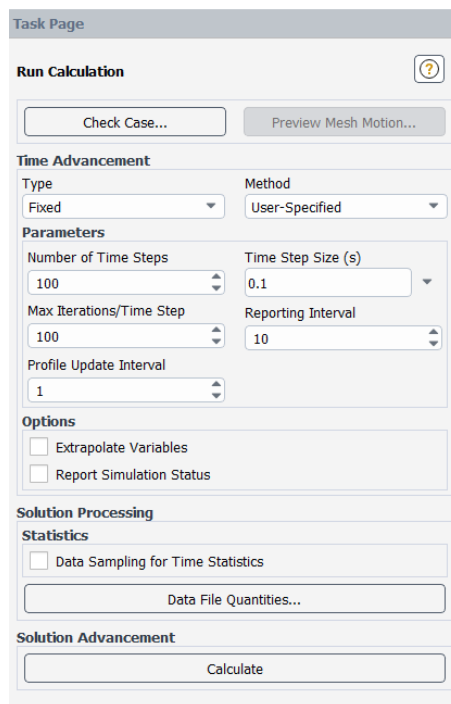


Figure 3.17: Calculation settings for the simulation

3.4.8 Drag Calculation Methods

The primary factor affecting the times of the kayaker are the drag inefficiencies which act opposite to the forward motion. The skin friction drag, and pressure drag will be the most important outputs of the simulations, and an understanding of them will be most important in being able to create a competitive advantage. To find these drag outputs, monitors for the above water and below water sections of the kayaker were set in Section 3.4.7. The parameter output however does not entirely determine the phase causing the drag, merely if it is caused above or below the waterline. As the water rises and falls, the drag due to each fluid will differ in respect to the waterline on the XZ plane.

The post processing results menu also features a drag calculator, which can be used at any time step desired of the transient simulation. It does allow the drag to be isolated the different phases at a particular time step. An example of the drag calculator found in post processing is shown in Figure 3.18. As all results are compiled over the variety of wind speeds, plots will be made to shows the relationship between wind speed, kayaker speed and drag force.

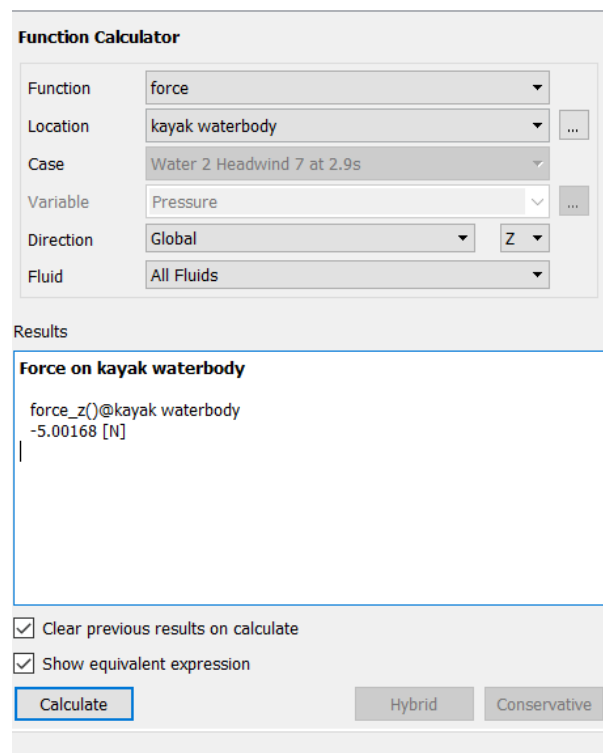


Figure 3.18: Drag Calculation Method found in post processing.

3.5 Chapter Summary

The preliminary simulation identified a number of requirements for the main project simulation which were not thought of previously. CFD software contains a huge amount of options when deciding which methods to use and why. The ANSYS fluent user guide was used heavily in assigning the best methods of recreating the kayaking system.

Chapter 4

Results

4.1 Chapter Overview

The results section contains the simulation drag outputs, both numerical and visual. The tables and graphs within this section show the drag increases at different kayak velocities, as well as the effect of wind on drag through headwind and wave simulations. The results are split into the sections: no wind; low velocity; racing velocity; and small waves.

4.2 Simulation Outputs

A total of 88 simulations were carried out and the drag forces above and below the originally waterline were stored in a parameter set. The above and below waterline figures would change depending on the wind speed and its effect on the water level, as well as the air and its own aerodynamic drag. Therefore, only the total drag was considered for analysis. When further clarification was required, it was possible to identify which phase is causing the drag at any specific time by accessing the calculator in the post results, as shown previously in Figure 3.18.

4.2.1 Convergence

The solution set convergence for all parameters at $1e^{-4}$, and all simulations met this requirement, visible in the monitor and messaged in the console. The residuals tended to move in a zig-zag pattern throughout the simulations, particularly for the second order and PISO solving method when compared to the default SIMPLE and first order settings. For the basic geometries created, the convergence figured were considered adequate, however this will need increasing to $1e^{-5}$ or $1e^{-6}$ as the geometry becomes more complex. A typical monitor of the scaled residuals is shown in Figure 4.1.

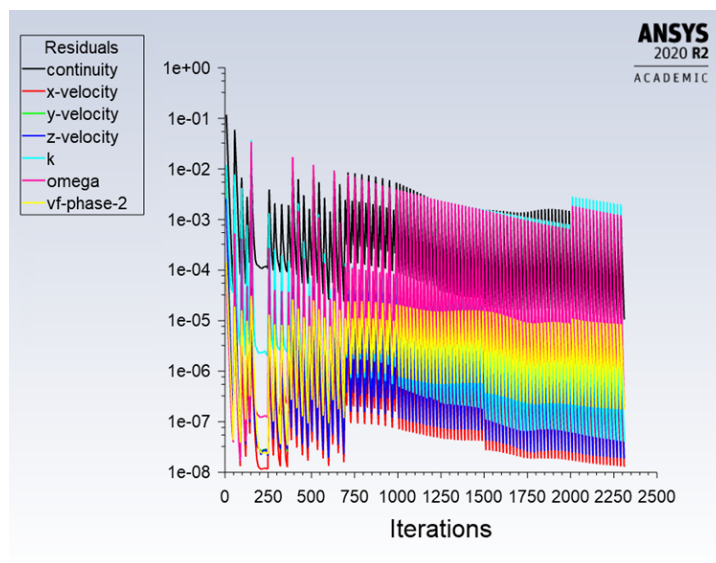


Figure 4.1: Typical Residual Report for Simulations

4.2.2 yPlus Value

The yPlus value of the model indicates the suitability of the mesh size for the simulation. Due to meshing constraints, the yPlus is relatively high for this model, at a maximum of approximately 3000 within the water domain, with most of the air enclosed geometries less than 250.

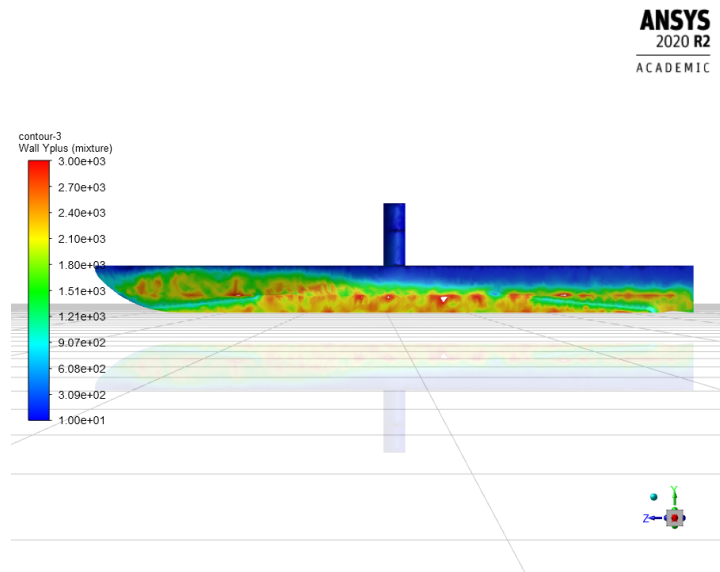


Figure 4.2: Contour of Yplus for 6m/s, ranged from 10 - 3000

4.3 Project Simulation

4.3.1 No wind Results

The initial simulations attempted used the open channel flow with no additional wind speed, establishing the baseline for open channel flow and determining the water surface without the interaction of wind. Figure 4.3 shows the deflection of the water around the hull at a water inlet boundary condition of 2m/s. The changes in colour of the vectors indicate a velocity change in the fluid; the lighter colour vectors indicate a slowing of the fluid, and the orange free stream vectors show the initial speed of 2m/s. Figure 4.3 also gives a good indication of the boundary layer by the deflection of the streamline away from the kayak hull.

4.3.2 Baseline Simulations

The baseline simulations were created with an inlet air speed equal to the inlet water speed, to create a simulation of a static day with no headwind applied to the kayaker.

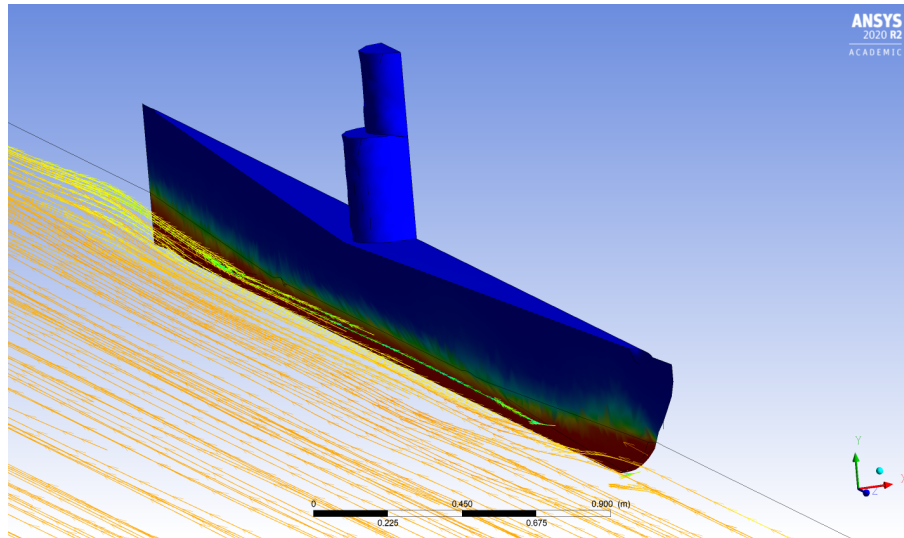


Figure 4.3: Vector of the water's surface, showing change in velocity.

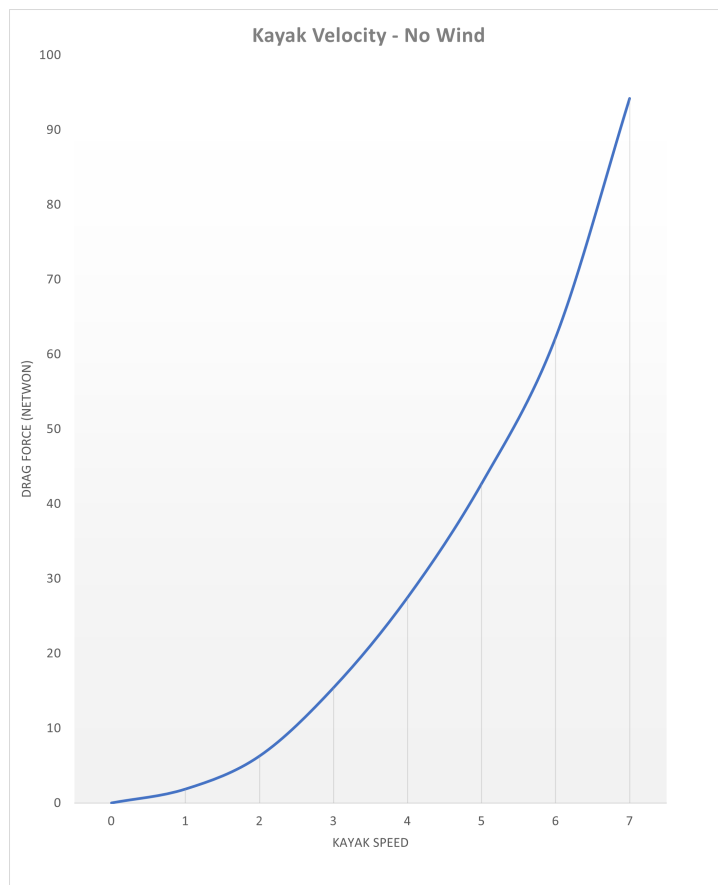
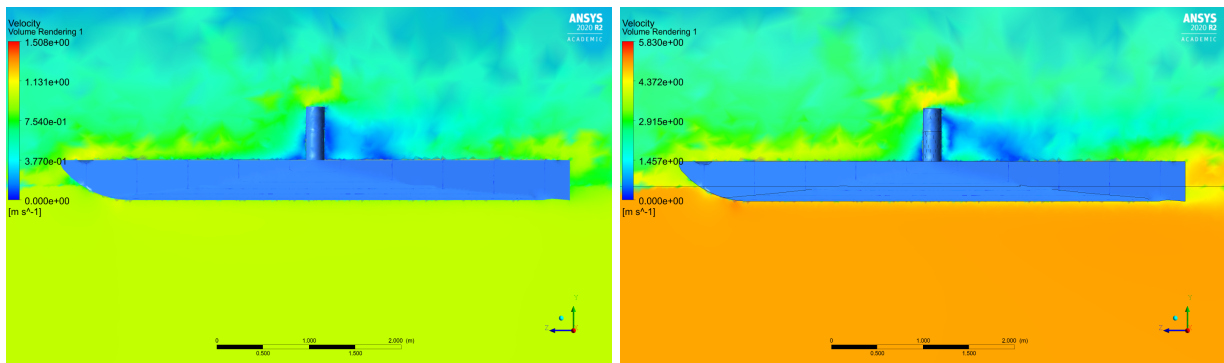


Figure 4.4: Drag Force Vs Kayak Speed - No Wind present.

Table 4.1: Drag Forces found with no wind applied to simulation

Waterspeed	Airspeed	Drag Force (N)
1	1	1.861
2	2	6.278
3	3	15.415
4	4	27.486
5	5	42.703
6	6	62.224
7	7	94.211

Figure 4.5 shows a volume rendering for the changes in velocity for comparison of 1m/s and 5m/s kayaker. Although the rendering is three-dimensional, the velocity change of air as a result of drag is visible. Figure 4.6 shows similar results as vectors placed on streamlines for the air domain.



(a) Velocity Changes of Air for 1m/s velocity

(b) Velocity Changes of Air for 5m/s velocity

Figure 4.5: Volume Rendering of the Velocity of fluids for a 1m/s and 5m/s kayaker

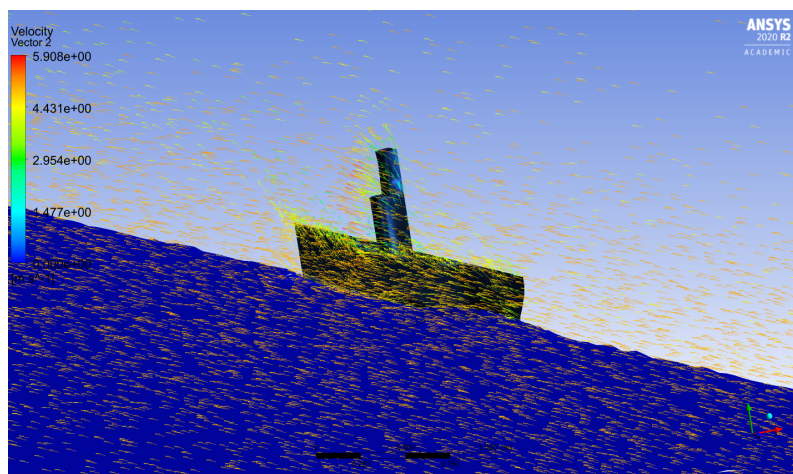


Figure 4.6: Air Velocity changes shown with Vectors for 5m/s velocity air.

4.3.3 Low-speed with Headwind

The next set of simulations were carried out for kayak speeds between 1m/s-3m/s. For each speed, headwinds ranging from 1-10m/s were applied and the drag force calculated. The kayak speeds tested here are likely to be lower than the racing speed, however their results help to understand the fundamental relationship of kayaker velocity versus drag force.

The simulation results are shown in tables 4.2, 4.3 and 4.4 with the drag force a sum of the above and below waterline drag forces. The drag increase is relative to the simulation for that kayak speed without any headwind present.

Table 4.2: Drag Forces for a Kayaker at 1m/s with increasing headwinds

Waterspeed	Headwind	Drag Force (N)	Drag Increase (%)
1	1	1.861	0.76
1	2	1.875	2.72
1	3	1.911	4.22
1	4	1.939	7.73
1	5	2.004	12.75
1	6	2.098	19.28
1	7	2.219	29.49
1	8	2.409	44.92
1	9	2.696	63.38
1	10	3.040	83.63

Table 4.3: Drag Forces for a Kayaker at 2m/s with increasing headwinds

Waterspeed	Headwind	Drag Force (N)	Drag Increase (%)
2	1	6.430	0.76
2	2	6.454	1.13
2	3	6.465	1.30
2	4	6.531	2.33
2	5	6.657	4.16
2	6	6.862	7.52
2	7	7.100	11.25
2	8	7.352	15.20
2	9	7.631	19.58
2	10	7.955	24.65

Table 4.4: Drag Forces for a Kayaker at 3m/s with increasing headwinds

Waterspeed	Headwind	Drag Force (N)	Drag Increase (%)
3	1	15.00	0.56
3	2	15.03	0.83
3	3	15.10	1.24
3	4	15.25	1.73
3	5	15.43	2.28
3	6	15.65	2.83
3	7	15.90	3.43
3	8	16.13	4.51
3	9	16.40	5.38
3	10	16.70	6.19

The results show the largest percentage increase of drag for the slowest kayak speed tested of 1m/s, with an 83.63% increase in drag for the 10m/s headwind, for a total 1.18N increase relative to no wind. For the 2m/s simulations, this difference was a 24.65% increase for a 1.68N drag increase, and 3m/s found a 6.19% increase with a 1.7N resistance.

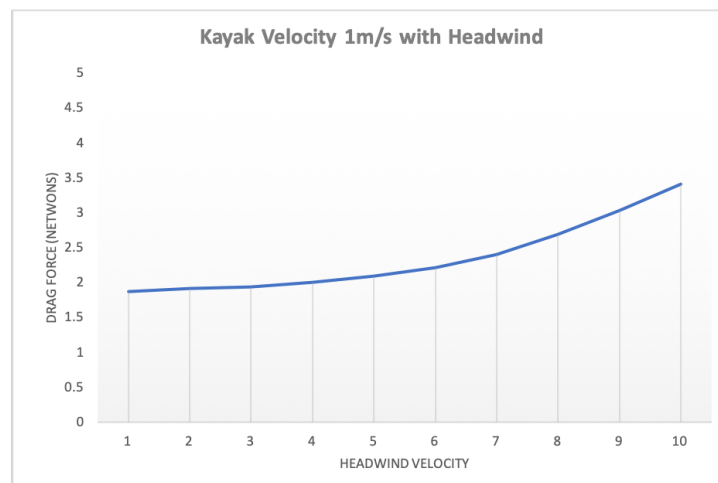


Figure 4.7: Drag Force Vs Headwind Speed - Kayak Velocity 1m/s

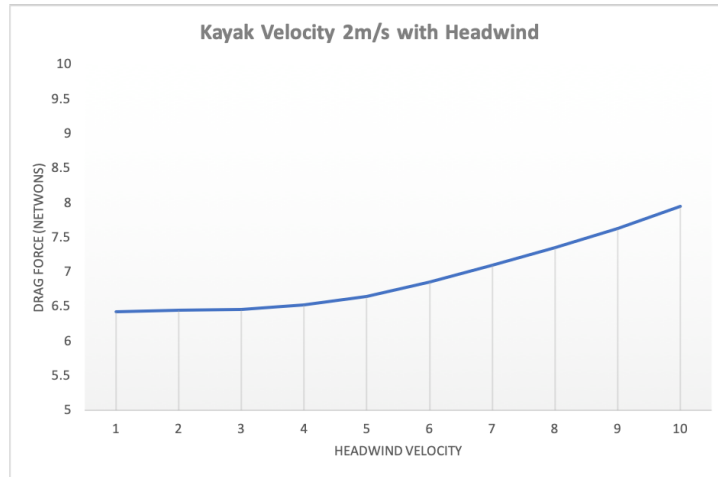


Figure 4.8: Drag Force Vs Headwind Speed - Kayak Velocity 2m/s

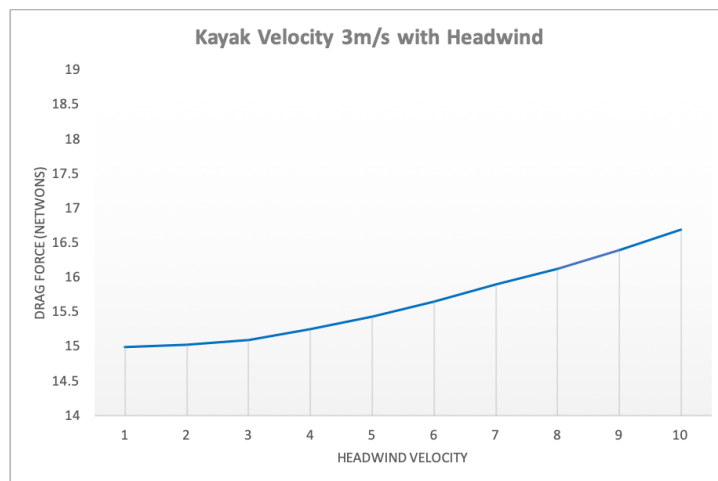


Figure 4.9: Drag Force Vs Headwind Speed - Kayak Velocity 3m/s

4.3.4 Racing Velocities with Headwind

The simulations for the low-speed simulations were repeated for speeds between 4-7m/s. These speeds cover the race pace of a kayaker during competition, and are more pertinent to the aims of the project. The tables 4.5-4.8 and graph figures 4.10-4.13 are presented, showing the drag force relative to headwind for each of the kayak speeds. The percentage drag increase for each simulation, relative to no wind, is included in each table.

Table 4.5: Drag Forces for a Kayaker at 4m/s with increasing headwinds

Waterspeed	Headwind	Drag Force (N)	Drag Increase (%)
4	1	27.35	0.27
4	2	27.43	0.47
4	3	27.53	0.94
4	4	27.67	1.94
4	5	27.82	3.15
4	6	27.97	4.63
4	7	28.13	6.26
4	8	28.43	7.84
4	9	28.66	9.63
4	10	28.88	11.58

Table 4.6: Drag Forces for a Kayaker at 5m/s with increasing headwinds

Waterspeed	Headwind	Drag Force (N)	Drag Increase (%)
5	1	42.20	0.12
5	2	42.20	0.12
5	3	42.30	0.35
5	4	42.42	0.65
5	5	42.62	1.11
5	6	42.86	1.69
5	7	43.14	2.34
5	8	43.45	3.09
5	9	43.85	4.03
5	10	44.19	4.83

Table 4.7: Drag Forces for a Kayaker at 6m/s with increasing headwinds

Waterspeed	Headwind	Drag Force (N)	Drag Increase (%)
6	1	60.68	0.00
6	2	60.70	0.03
6	3	60.75	0.11
6	4	60.90	0.37
6	5	61.17	0.80
6	6	61.51	1.37
6	7	61.92	2.05
6	8	62.45	2.92
6	9	63.15	4.08
6	10	63.84	5.20

Table 4.8: Drag Forces for a Kayaker at 7m/s with increasing headwinds

Waterspeed	Headwind	Drag Force (N)	Drag Increase (%)
7	1	91.16	0
7	2	89.91	-1.38
7	3	89.40	-1.93
7	4	89.20	-2.15
7	5	89.19	-2.16
7	6	89.23	-2.11
7	7	89.34	-1.99
7	8	89.62	-1.70
7	9	90.17	-1.08
7	10	90.58	-0.63

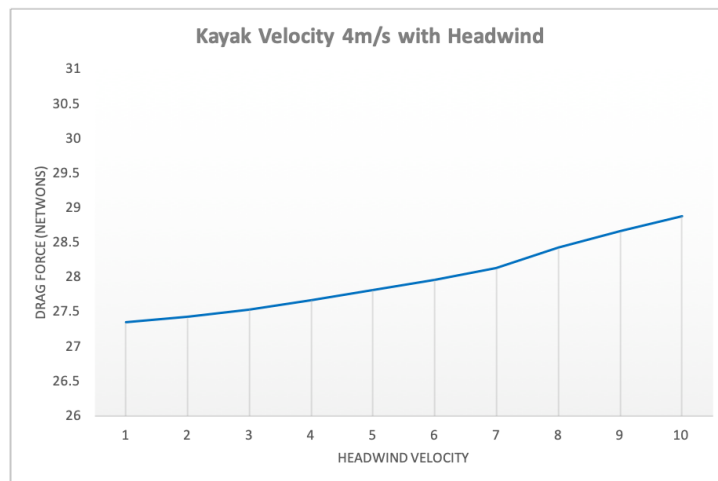


Figure 4.10: Drag Force Vs Headwind Speed - Kayak Velocity 4m/s

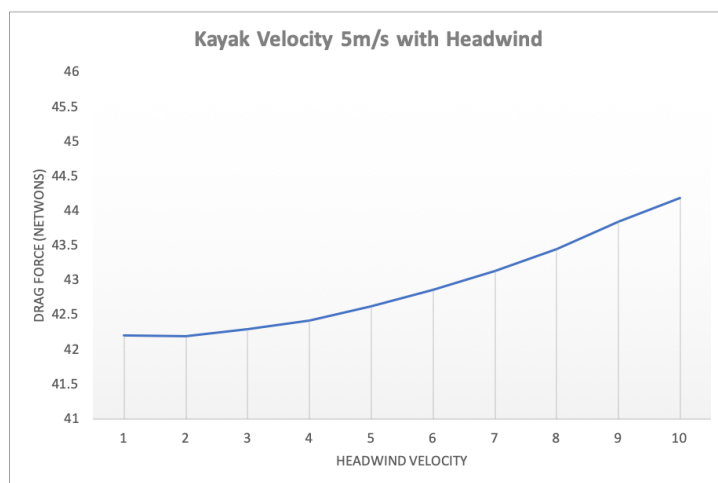


Figure 4.11: Drag Force Vs Headwind Speed - Kayak Velocity 5m/s

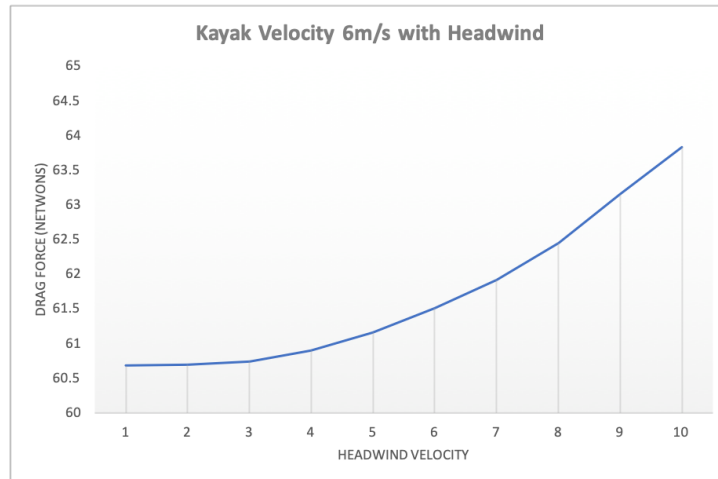


Figure 4.12: Drag Force Vs Headwind Speed - Kayak Velocity 6m/s

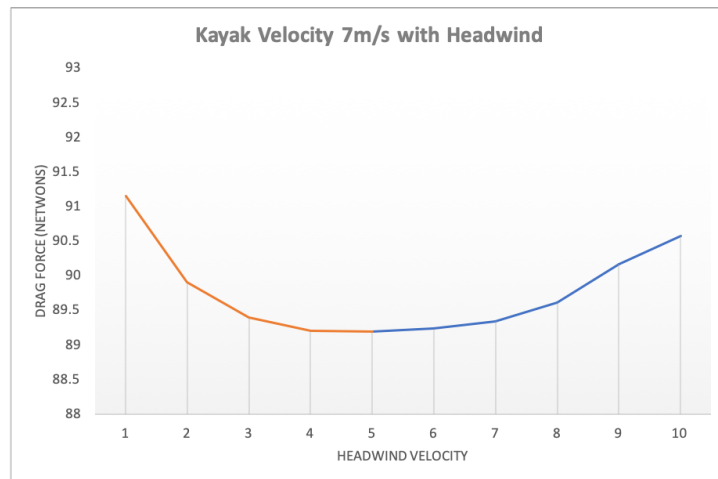
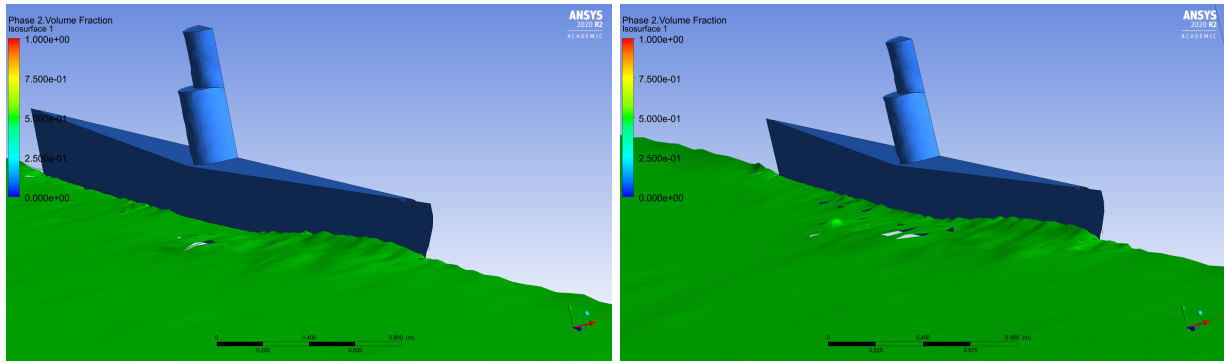


Figure 4.13: Drag Force Vs Headwind Speed - Kayak Velocity 7m/s

The percentage drag increases for the simulations were 11.58%, 4.83%, 5.20% and -0.63% for respective kayak speeds from 4-7m/s. The decreases of drag found in the 7m/s simulation is considered a limitation of the model and is discussed further in chapter 5.

4.3.5 Racing Velocities with Headwind and Waves

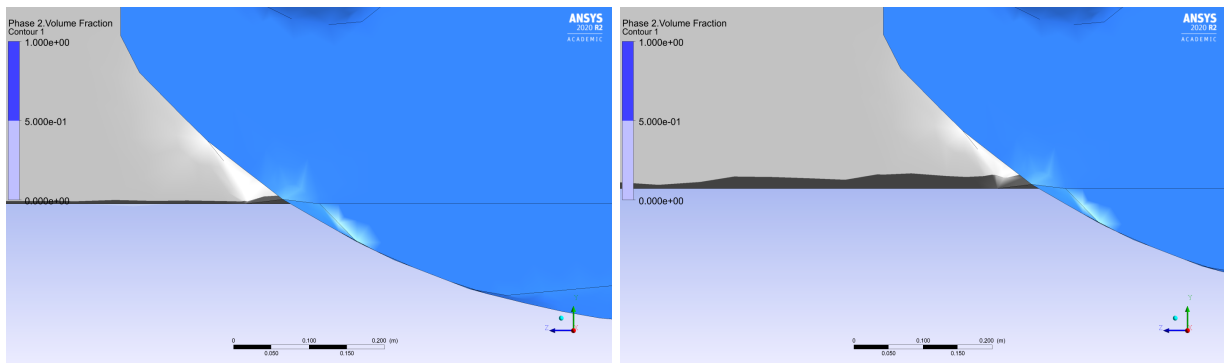
The final simulation attempted created small waves, similar to those visible on a river on a windy day, to record the drag changes due to this effect. Figures 4.14 and 4.15 shows the slightly larger bow wave created with the wave boundary condition applied.



(a) Simulation of 5m/s without Waves

(b) Simulation of 5m/s with Waves

Figure 4.14: Small Wave Effect on Bow Wave created by Kayak



(a) Simulation of 5m/s without waves

(b) Simulation of 5m/s with Waves

Figure 4.15: Small Wave Effect on Water Surface close to Kayak

The simulations found increased drag for the wavy conditions at all speeds from 4-7m/s. Speeds lower than this were not tested as it was deemed unlikely winds lower than these speeds would create any waves on the water’s surface.

The drag was higher for all wave simulation tested. It was noticed that the above waterline drag figures increased while the below waterline figures decreased. The approximate percentage drag increase was between 5-6% for the speeds tested, as shown in Figure 4.16.

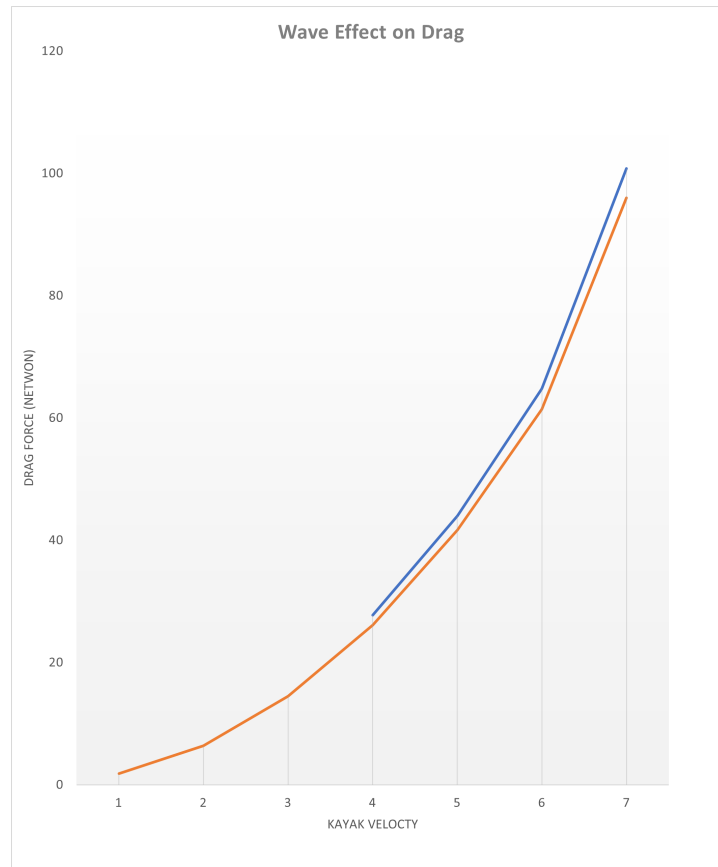


Figure 4.16: Drag Comparison of Wave Effect Vs Flat water Simulations

4.4 Chapter Summary

This chapter communicated the drag outputs from the simulations, and compared the drag increases as a result of headwinds and small waves. The results were mostly consistent with expectations, and make sense when relating to the literature reviewed. There were some inconsistencies noticed in the high velocity simulations, which will be discussed in the next chapter.

Chapter 5

Discussion

5.1 Chapter Overview

This section interprets the results found in chapter 4 and relates the findings to the aims of this project. Whilst the simulation shows potential for the use in water-based sports, the results require validation and refinements to the model are required.

5.2 Simulations Results

The largest component of drag for the kayaker was the resistance through the water, both as parasitic drag and wave drag resistance. This was expected, as the density of water is approximately 800 times less than air, dependant on the temperature and pressure of each. Of the components of parasitic drag, it is suspected that skin friction drag is dominant for the kayak due to its quite low frontal area in comparison to its surface area. This is opposite for the athlete, where the frontal area is relatively large and flat. The simulation does not differentiate the different mechanisms, only the force opposing motion, so therefore further analysis would be required if this information was of interest.

The drag figures for the open channel simulations, without additional headwind, shows an exponential increase in drag with a linear increase in velocity. This reflects the research by showing that the drag coefficient is a function of the fluid velocity at a particular Reynolds number, which

in itself is a function of velocity. The results for all seven kayak speeds shown previously in Results Figure 4.4, plotting drag against velocity for n . The 2nd order trend line for the data input into Microsoft Excel was found as:

$$D_F = 2.15\vec{V}^2 - 6.47\vec{V} + 5.43 \quad (5.1)$$

with drag being a function of velocity. From this equation it can be seen as the kayaker velocity increases, the drag force approaches $2.2\vec{V}^2 - 6.5\vec{V}$, with the residual third term becoming less significant. Further data points and higher order equations would improve the accuracy and validate this trend. As the simulation contained no headwind, the drag increase for this parameter set is due to the travel of the kayak through the water and a simulated static air, with no dynamic headwind.

Overall the simulations carried out went towards proving the viability of using CFD to recreate the drag conditions of a kayaker. However, the simulation was limited in by a number of factors, and as the boundary conditions increased, the confidence in the accuracy of the models became lower. For example, the 7m/s kayaker encountering headwinds actual registered less drag for headwinds from 1-5m/s than the no wind condition. This is the not able to be explained from an understanding of the drag mechanisms, and inconsistent with the lower kayak velocities.

5.3 Geometry

The final hull and athlete kayak geometry created was basic in shape, and the drag figures found in the simulation are unlikely to be highly accurate of the figures found in real life. The simulation does however provide enough information for trend analysis and the distribution of the drag over a real kayaker. The shape was limited by the mesh, with draft versions containing arms and a paddle proving extremely difficult to interface with the mesh of the free stream fluid paths. This is easily fixed with the availability of more meshing elements, and the domain design of the two-phase model would lend itself well to other water sport geometries conducted on flat water.

5.4 Meshing

The meshing process identified the areas of most interest, being the water/air interface surface and the walls of the kayaker, and attempted to create as fine as possible mesh in these areas. The limitation of the meshing elements available in the student version did not allow for the mesh to reach a high degree of accuracy, however the solutions were able to converge and provided data which could be analysed.

The $yPlus$ figures increased as the fluid velocities increased, further raising the concern for inaccuracy as the inlet boundary condition magnitudes increased. The importance of the $yPlus$ is most applicable to skin friction and the creation of the boundary layer, and is likely most important for the hull of the kayak, where the frontal area is quite low. The large frontal area of the kayaker's body and the dominance of pressure drag for this section would allow for an increase the allowance of $yPlus$ for this region. Figure 5.1 shows a contour of $yPlus$ for a 6m/s kayak, and the areas outside of the range on this figure would require mesh refinement. In particular the sections of the kayak travelling in the water domain. This was limited in this project due to the cap on meshing elements available in the academic version.

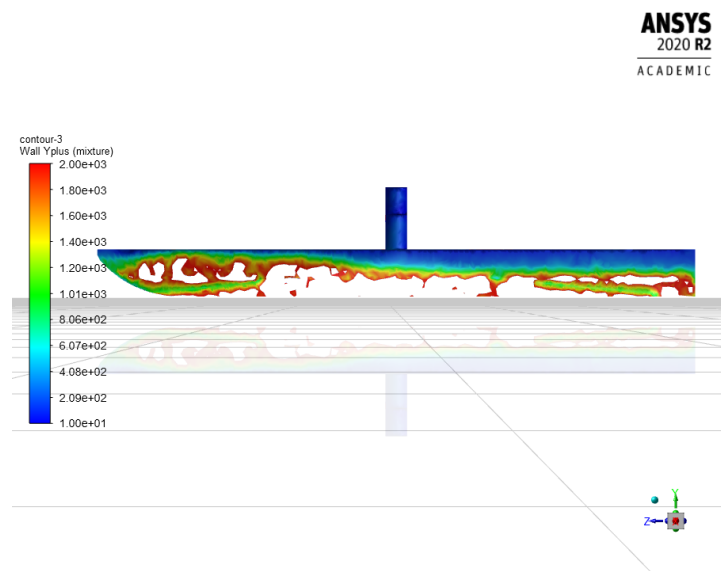


Figure 5.1: Contour of $Yplus$ for 6m/s

5.5 Wave Creation

The use of the Volume of Fluid multiphase inlet boundary condition allowed for the creation of waves over the water inlet, and was used to simulate the small waves which would be found on a body of water on a windy day. Ideally, the small waves would be best modelled by creating a very fine mesh interface and setting up an accurate surface interaction between the air and the water. Due to the size of the domain and the meshing restrictions this preferred option was not possible.

5.6 Effects of Wind

The simulations investigated the effect of wind in two ways: through headwind on flat water; and by creating small waves reflecting the shear stress of the wind on the water. From the results, it was found that the waves had a larger effect on drag than even the 10m/s headwind at kayak speeds of 6m/s and greater, and greater than a 9m/s wind at 5m/s kayak velocity. Competition is unlikely to be conducted at these headwind speeds, which suggests that the primary effect of wind on kayakers is through hydrodynamic drag through the waves created by the shear stress imparted by the wind on the water's surface.

5.7 Pacing Strategy

The results provided insight into the types of increases of drag above at higher velocities. One example of how these results can be applied to competition would be to compare pacing strategies of actual races. The 2018 World Championship was won with a time of 207.66 seconds (*ICF: Kayak 2020*), which is shown in table 5.1 along with the 250m split times.

Table 5.1: World Championship Final Times

Intervals (m)	Splits (secs)	Avg Velocities (m/s) (%)
250	48.503	5.15
500	101.104	4.75
750	154.576	4.68
1000	207.666	4.71

The common pacing strategy used by competition kayakers is referred to as the reverse J strategy, which includes an all-out start before settling for an even pace, before a slight burst towards the end. This is reflected in the previous table, and shown in figure 5.2a as the blue line. From the simulations it was apparently that the cost of increased kayak velocity is a larger increase of drag, and therefore accelerations and higher velocities require increased effort. It was proposed that an even pacing strategy for the same winning time would be more efficient.

Simulations were created for the average velocity of even pacing strategy and each average velocity of the reverse J strategy, and drag outputs taken. The comparison of reverse J strategy and even pacing strategy is shown in figure 5.2.

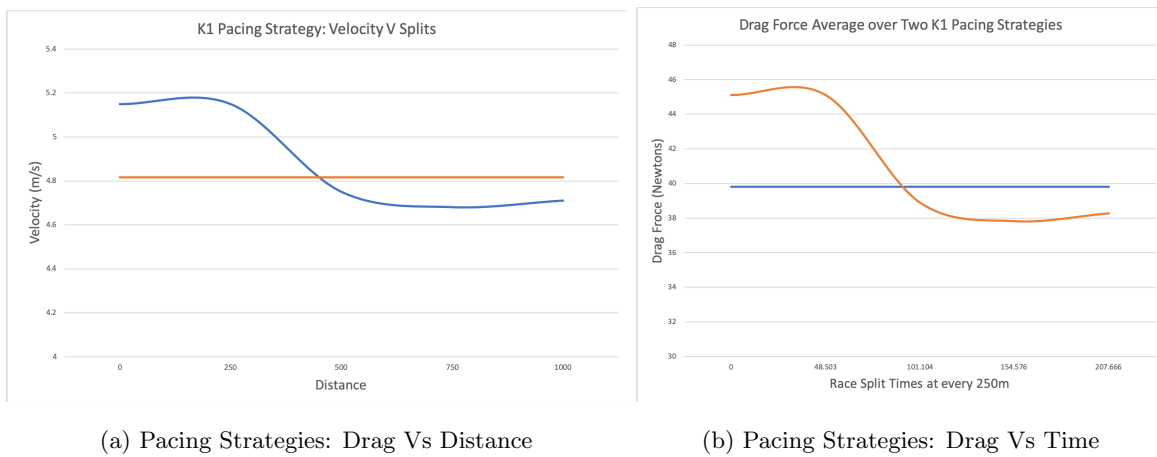


Figure 5.2: Comparison of Pacing Strategies for 2018 WC final

From the drag outputs the work for each strategy was calculated from:

$$W_{min} = F_D * \vec{V} * (t_1 - t_0) \quad (5.2)$$

and it was found that the even pacing required 210.8 Joules less. This efficiency saving could be applied to a slightly higher average race pace, and a faster time achieved for the same energy as the reverse J method. Not all variables were tested by this method, as the initial accelerations were not included as well as the deceleration shown in the reverse J method. The simulations were also without headwind, which would likely increase the advantage of the even pacing technique.

From research of the literature, the reasons for the reverse J strategy were listed as possibly providing $\dot{V}O_2$ max advantages as well as avoiding boat wake of others. It may also be psychological.

However, the efficiency of this method in regards to drag is lower, and warrants a cost-benefit analysis in real world conditions.

5.8 Chapter Summary

The use of the simulations to provide pacing strategies shows promise, however requires validation. The accuracy of the current model is slightly concerning, especially at high velocities. This is due to the meshing and geometry limitations currently existing within the project. This chapter provided points of improvement possible explanations for some of the inconsistencies noticed in the results.

Chapter 6

Conclusions and Further Work

6.1 Conclusion

The effect of wind on drag on kayakers in competition was tested by the creation of an ANSYS Fluent CFD model with variable headwinds and waves. The model featured a dual inlet, which allowed individual adjustment of water and air speed to separate kayak velocities and head winds.

Section 1.3 details the aims of the project. A summary of these goals and how they were addressed are as follows:

Conduct Research on the movement of the kayak through the water: Chapter 2 completed a literature review of the drag mechanisms of the kayaker through water and air. The kayaker encounters three types of drag: Form drag; Friction drag; and Wave Drag Resistance.

Research CFD methods and their application CFD techniques, particularly those found in ANSYS Fluent, were researched in Chapter 2. The research identified the suitability of the Volume of Fluid model, combined with an SST $k-\omega$ with standard wall functions to model turbulence.

Create a simple model of a body of water, determining the impact of wind: This goal was partly achieved through the preliminary simulations found in Section 3.3. The full intention of this goal was to accurately simulate the water's surface through the CFD model alone, however this was unable to be carried out, as discussed in Section 5.6. This goal was

instead met by the use of the wave inlet boundary condition within the Volume of Fluid model.

Determine Drag on an object within CFD: The preliminary simulations in Section 3.3 achieve drag outputs for a cylinder, and the project simulations in Section 4.3 applied these methods to achieve the project aim.

Create a kayak model and analysis drag outputs: The final model consisted of a dual inlet domain for a multiphase model, which created a parameter set of the drag outputs for above and below the initial waterline. Section 4.3 details the methodology used, the Chapter 4 details the results and the discussion of these findings is found in Chapter 5.

Provide feedback on results and methods for better race times: The results of the drag outputs are shown in Chapter 4 and discussed in 5. The results provided useable data for speeds up to 6m/s, however as the velocities increased beyond this the confidence in the results lessened. The application of the model and the results was provided in Section 5.7, where the 2018 World Championship winning strategy versus an even pacing strategy, and it was found that the even pacing strategy was more energy efficient by 210.8 Joules.

6.2 Further Work

6.2.1 Model Refinements

The model shows potential as being a way to simulate water and wind in a single model for CFD analysis of water sports conducted on flat water. The simulation requires definite refinements in a number of areas:

Geometry: The geometry is currently quite rough, and not accurate to the dimensions of a kayak hull or athlete. Further work can be carried out by selecting a particular kayak hull and creating a 3D model to within a low tolerance limit. The materials of the hull were also not changed, and the effect of the different kayak composite materials and its effect on drag is another point of further research.

Mesh: As mentioned in discussion, the limitation of meshing elements on the academic version of the ANSYS Fluent software did not allow for high level of accuracy on the model. If

a licenced software version is available, then mesh refinements of the waters surface and kayaker's frontal area would be a priority. Another body of influence should be created purely around the area of water/air interaction, fine enough to allow for waves induced by the wind as well as bow waves from the kayak. This mesh would need to be very fine to try and simulation the water's surface and the wind effects on it. The yPlus would need to be substantially reduced

Setup: The current residuals are converged to 1^{-4} for the current mesh, and with improvement to the geometry and mesh it is likely a highly level of convergence would be required to reach the accuracy expects.

6.2.2 Wave Creation

The magnitude of the waves created by a particular wind on a water's surface requires its own unique CFD model with an extremely find mesh created for the water's surface. The literature review provides equations for the wind effect on wave creation on the waters surface, however recreating this on the project was not possible due to meshing limitations and time restrains.

6.2.3 Practical Testing

Once the geometry and accuracy are refined, the results should be compared to practical testing in identical conditions. As an initial study, the wind effects on the waters surface should be conducted on various locations, to determine the impact of other variables on wave creation. The waters depth, current and width are all likely to change this.

Testing should then be conducted in either a wind tunnel or on a lake to determine the accuracy of the drag figures produced in Fluent. The preference would be for kayakers on water to incorporate wave drag resistance as well as hydrodynamic and aerodynamic drag. The research of the literature found that variable controlled experiments were able to be conducted by use of a cable system pulling the kayak and measuring the total resistance to forward motion. Headwinds are likely to be difficult to control outside of a wind tunnel, and this may be the best method of recreating the drag effects of headwind.

6.2.4 Expansion of Model

If the kayak simulation reaches a high level of accuracy there is scope to extend the model to other geometries used in other water sports. This is mentioned in the project aims as a stretch goal if time permitted. Other sports conducted on flat water are canoeing, paddle boarding, boating, skiing and jet skiing. Ultimately, this type of simulation may become part of athlete training through an Institute of Sport, to help analyse times and drag from events and determine strategies based on this data.

References

Anderson, J. D. (2013), 'Governing equations of fluid dynamics'.

URL: <http://www.eng.auburn.edu/~tplacek/courses/fluidsreview-1.pdf>

ANSYS (2020).

URL: <https://www.ansys.com>

ANSYS, I. (2013), 'Ansys fluent user's guide'.

Autodesk (2020), 'External incompressible flow'.

URL: <https://knowledge.autodesk.com/support/cfd/learn-explore/caas/CloudHelp/cloudhelp/2019/ENU/SiUsersGuide/files/GUID-4EED9E6E-A694-4505-9502-8D9CC42A5EC2-htm.html>

Barber, H. (2018), 'Effect of wind in the field of play for elite sprint kayakers', Ottawa-Carleton Institute for Mechanical & Aerospace Engineering.

Barros, F. (2015), 'Study of kayak hull design on calm water resistance', Faculdade de Engenharia da Universidade do Porto.

Bishop, D., Bonetti, D. & Dawson, B. (2002), 'The influence of pacing strategy on $\dot{V}O_2$ and supra-maximal kayak performance'.

Borges, T. O., Bullock, N. & Coutts, J. A. (2013), 'Pacing characteristics of international sprint kayak athletes', *International Journal of Performance Analysis in Sport* **13**(2), 353–364.

Brennen, C. (2018), *An Internet Book on Fluid Dynamics - Wave Drag*, California Institute of Technology.

URL: <http://brennen.caltech.edu/fluidbook/externalflows/drag/wavedrag.pdf>

Canoeing at the Summer Olympics (2020), Wikipedia Contributors.

Canoe/Kayak: Hydrodynamics (2020), Encyclopedia Britannica.

URL: <https://www.encyclopedia.com/sports/sports-fitness-recreation-and-leisure-magazines/canoekayak-hydrodynamics>

Chanson, H. (2004), *The Hydraulics of Open Channel Flow: An Introduction*, 2 edn, Elsevier.

Connor, N. (2019), 'What is skin friction – friction drag – definition'.

URL: <https://www.thermal-engineering.org/what-is-skin-friction-friction-drag-definition/>

Dawson, C. & Mirabito, C. (2008), 'The shallow water equations'.

URL: <https://users.oden.utexas.edu/arbogast/cam397/dawson>

Drag (Physics) (2020), Wikipedia Contributors.

URL: [https://en.wikipedia.org/wiki/Drag_\(physics\)](https://en.wikipedia.org/wiki/Drag_(physics))

Fang, C., Yang, R. & Shugan, I. (2011), 'Kelvin ship wake in the wind waves field and on the finite sea depth', *Journal of Mechanics* **27**, 71 – 77.

Feldmeier, A. (2019), *Theoretical Fluid Dynamics*, Springer.

Fleming, N., Donne, B., Fletcher, D. & Mahony, N. (2012), 'A biomechanical assessment of ergometer task specificity in elite flatwater kayakers', *Journal of Sports Science and Medicine* **11**(16-25).

Florek, S. (2012), 'Tentative chronology of indigenous canoes of eastern australia'.

URL: <https://australianmuseum.net.au/blog/science/tentative-chronology-of-indigenous-canoes-of-eastern-australia/>

Frei, W. (2017), 'Which turbulence model should i choose for my cfd application?', Comsol Blog.

URL: <https://www.comsol.com/blogs/which-turbulence-model-should-choose-cfd-application/>

Froude Number (2020), Encyclopedia Britannica.

URL: <https://www.britannica.com/science/Froude-number>

Gomes, B., Machado, L., Ramos, N., Conceiao, F., Sanders, R., Vaz, M., Vilas-Boas, J. & Pendergast, D. (2017), 'Effect of wetted surface area on friction, pressure, wave and total drag of a kayak', *Sports Biomechanics* .

Hall, A. (2015a), 'The drag equation', National Aeronautics and Space Administration.

URL: <https://www.grc.nasa.gov/WWW/k-12/airplane/drageq.html>

- Hall, A. (2015b), ‘Navier-stokes equations’, National Aeronautics and Space Administration.
URL: <https://www.grc.nasa.gov/www/k-12/airplane/nseqs.html>
- Henningson, D. & Berggren, M. (2005), ‘Fluid dynamics: Theory and computation’, KTH Royal Institute of Technology.
- ICF: *Kayak* (2020), International Canoe Federation.
- Kayak* (2020), Wikipedia Contributors.
URL: <https://en.wikipedia.org/wiki/Kayak>
- Mantha, V., Silva, A., Marinho, D. & Rouboa, A. (2013), ‘Numerical simulation of two-phase flow around flatwater competition kayak design-evolution models’, *Journal of Applied Biomechanics* **29**, 270–278.
- Michael, J., Rooney, K. & Smith, R. (2008), ‘The metabolic demands of kayaking: A review’, *Journal of Sports Science and Medicine* **7**, 1–7.
- Muller, M., Stam, J., James, D. & Thurey, N. (2008), ‘Real time physics class notes’, ETH Zurich.
- NuclearPower (2020), ‘Form drag - pressure drag’.
URL: <https://www.nuclear-power.net/nuclear-engineering/fluid-dynamics/what-is-drag-air-and-fluid-resistance/>
- Pelikan, P. & Markova, J. (2013), ‘Wind effect on water surface of water reservoirs’, *ACTA Universitatis Agriculturae et Silviculturae Mendelianae Brunensis* **61**(6), 1823–1828.
- Pendergast, D., Bushnell, D., Wilson, D. & Cerretelli, P. (1989), ‘Energetics of kayaking’, *European Journal of Applied Physiology* **59**, 342–250.
- Perfected-Flight (2020), ‘The truth about “induced drag”’, Perfected-Flight.
- Peric, M. & Ferguson, S. (2005), The advantage of polyhedral meshes, Technical report, CD-adapco.
- Pinkerton, P. (2017), ‘History of the canoe’, Web Article.
- Pritchard, P. & Mitchell, J. (2015), *Introduction to Fluid Mechanics*, 9 edn, John Wiley and Sons Inc.
- Robinson, M. G., Holt, L. E. & Pelham, T. W. (2002), ‘The technology of sprint racing canoe and kayak hull and paddle designs’, *International Sports Journal* **6**(2), 68–85.

Ship Resistance (2020), Wikipedia Contributors.

URL: <http://en.wikipedia.org/wiki/Shipresistanceandpropulsion>

Singh, Y., Bhattacharyya, S. & Idichandy, V. (2017), 'Cfd approach to modelling, hydrodynamic analysis and motion characteristics of a laboratory underwater glider with experimental results', *Journal of Ocean Engineering and Science* **2**, 90–119.

Skybrary (2017), 'Form drag'.

URL: <https://www.skybrary.aero/index.php/Form-Drag>

Stenmark, E. (2013), On multiphase flow models in ansys cfd software, Master's thesis, Chalmers University of Technology, Goteborg, Sweden.

Szanto, C. (2014), 'Canoe sprint coaching manual: Level 2 and 3'.

URL: <https://www.canoeicf.com/sites/default/files/icfCspCoachesManualLevel23.pdf>

Taha, Z., Hassan, M. H. A., Majeed, A. P. A., Aris, M. A. & Sahim, N. N. (2013), 'An overview of sports engineering: history, impact and research', *Malaysian Journal of Movement, Health & Exercise* **2**, 1–14.

Trancossi, M. & Pascoa, J. (2018), 'A new dimensionless approach to general fluid dynamics problems that accounts both the first and second law of thermodynamics', *Mathematical Modelling of Engineering Problems* **5**(4), 331–340.

Transonic Flow (2020), NASA History.

URL: <https://history.nasa.gov/SP-367/chapt5.htm>

Vallis, G. (2019), 'Essentials of atmospheric and oceanic dynamics', Cambridge University.

URL: <https://www-cambridge-org.ezproxy.usq.edu.au/core/books/essentials-of-atmospheric-and-oceanic-dynamics/shallow-water-equations/44BDDC7A2ABAC4489F09B32CB74057D3/online-view>

Versteeg, W. & Malalaseker, W. (2007), *An Introduction to Computation Fluid Dynamics: The Finite Volume Method*, 2 edn, Pearson, Prentice Hall.

Wandel, A. (2020), 'Computational fluid dynamics', University of Southern Queensland.

Appendix A

Project Specification

ENG4111/4112 Research Project

Project Specification

For: Dean Long

Title: Simulation of the Effects of Wind on the Drag on Kayakers in Competition

Major: Mechanical Engineering

Supervisors: Assoc Prof Andrew Wandel

Dr Khalid Saleh

Sponsorship: N/A

Enrolment: ENG4111 – EXT S1, 2020

ENG4112 – EXT S2, 2020

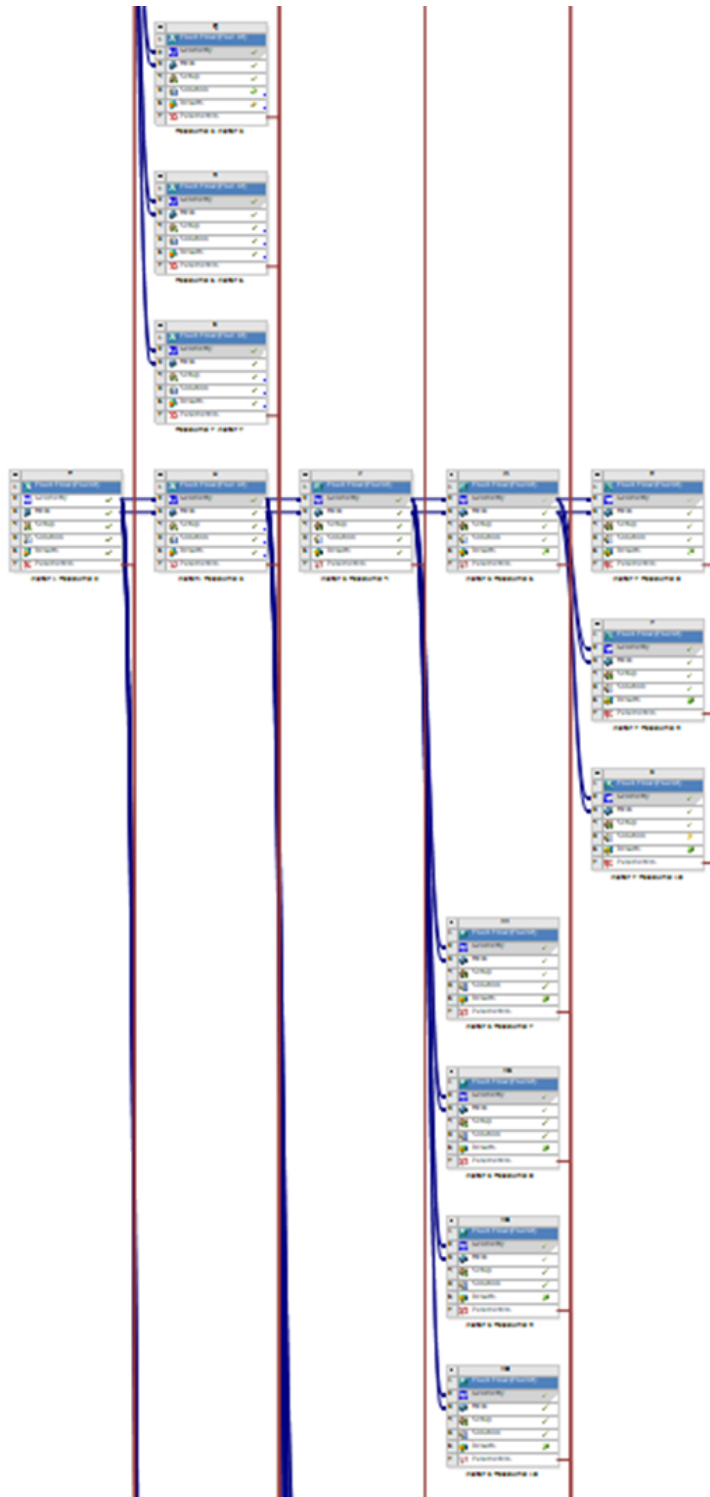
Project Aim: To create a simulation of competition kayakers competing in a range of wind conditions, affecting the aerodynamic drag and water surface. Examination of the results can identify sources of competitive advantage.

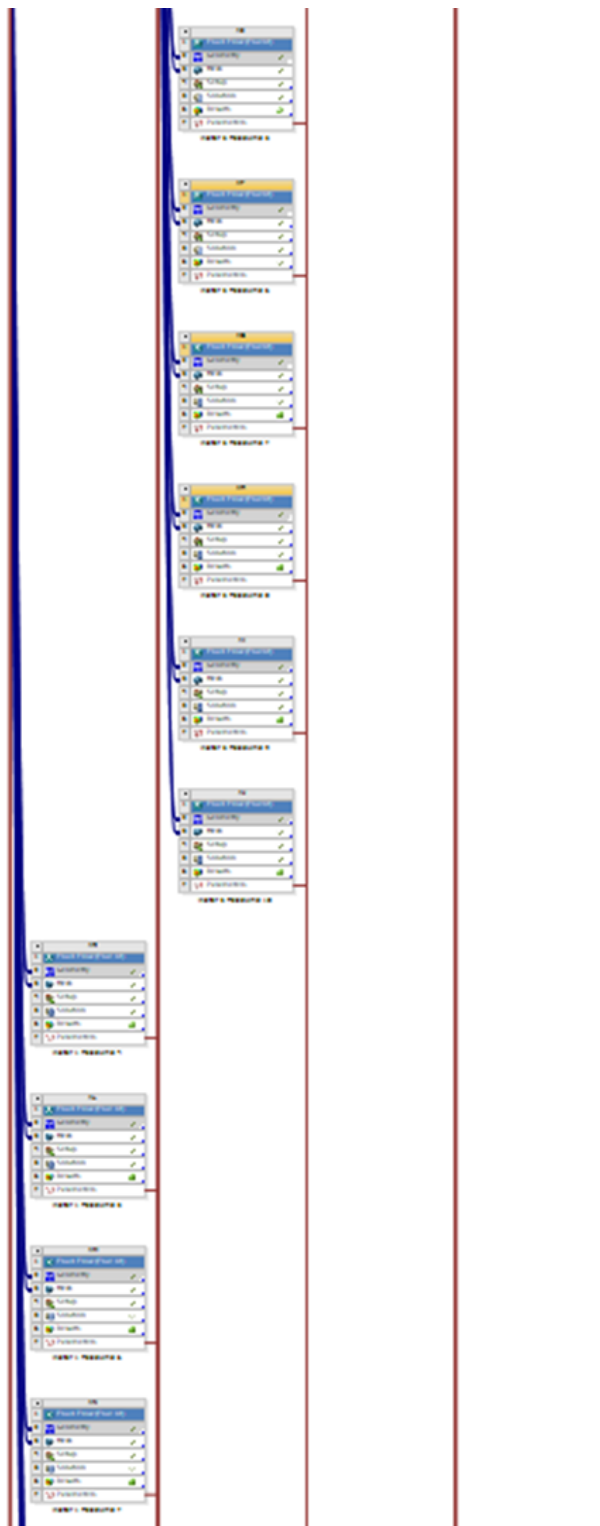
Programme: Version 1, 14 Mar 2020

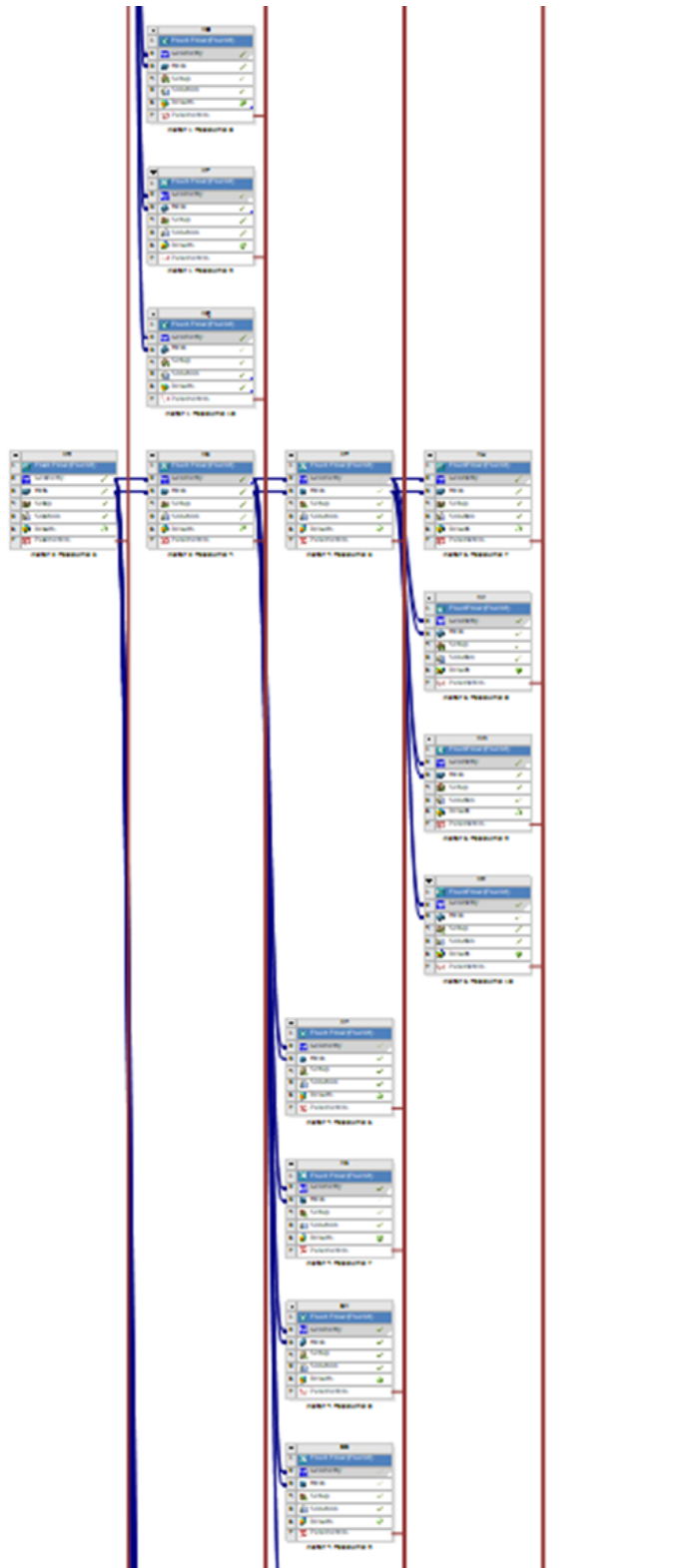
1. Review literature in regards to the drag forces encountered by Kayakers.
2. Detail the engineering theory behind the forces discovered in step 1, gaining an in-depth understanding of the drag forces and work that a kayaker produces.
3. Examine Computational Fluid Mechanics (CFD) methods for the use of water and wind within a single model.
4. Create a 3D model on CFD software that simulates the water surface affected by wind. Compare the simulation to previous wind-wave simulations and to videos of water bodies under known wind conditions.
5. Create a 3D model on CFD software of a kayaker moving through the water's surface, encountering drag from the wind and water surface. Validate the results to published literature on drag forces found on kayakers and other water athletes.
6. Extend model to vary the wind speed and direction, as both a head wind and tail wind. Validate the results against literature.
7. Compile the results found from the CFD software and compare to the theory discussed in step 2.

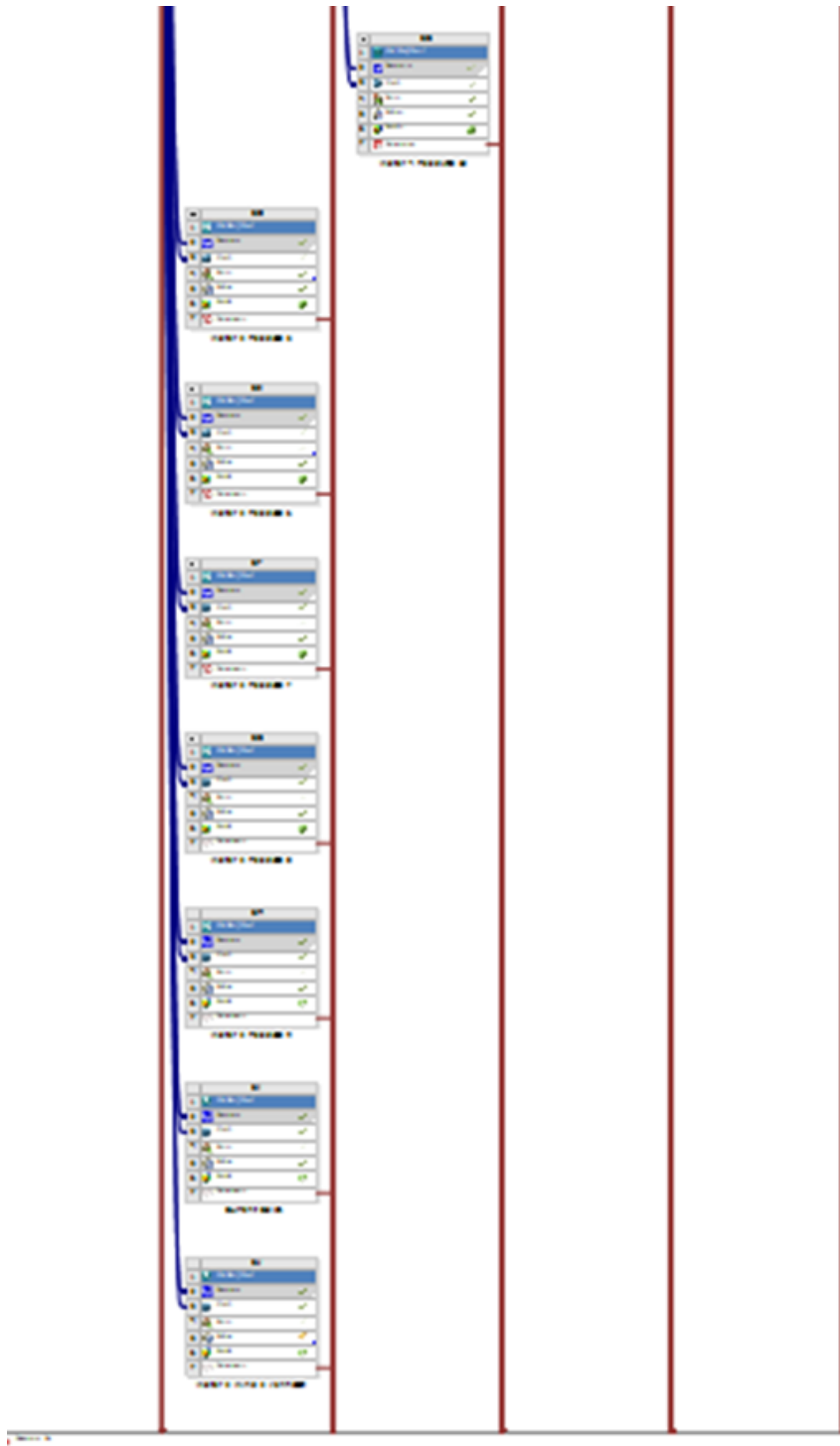
Appendix B

Fluent Outputs









B.2 Example of Parameter Set Output

KayakRedo - Workbench

File Edit View Tools Units Extensions Jobs Help

Project Parameter Set x

Update All Design Points

Outline of All Parameters

	A	B	C	D
1	ID	Parameter Name	Value	Unit
2	[-] Input Parameters			
*	New input parameter	New name	New expression	
4	[+] Output Parameters			
5	[+] Openchannel 1 (A1)			
6	P20	drag-waterbody-op	1.4915	N
7	P21	drag-coefficient-both-op	3.0142	
8	P22	drag-airbody-op	0.35472	N
9	[+] Openchannel 2 (B1)			
10	P23	drag-waterbody-op	5.7903	N
11	P24	drag-coefficient-both-op	10.419	
12	P25	drag-airbody-op	0.59142	N
13	[+] Water 5 and Waves, 0 wind (C1)			
14	P185	drag-waterbody-op	35.801	N
15	P186	drag-coefficient-both-op	71.804	
16	P187	drag-airbody-op	8.179	N
17	[+] Water 6 and Waves, 0 wind (D1)			
18	P194	drag-waterbody-op	50.916	N
19	P195	drag-coefficient-both-op	105.77	
20	P196	drag-airbody-op	13.867	N
21	[+] Water 7 and waves, 0 wind (E1)			
22	P197	drag-waterbody-op	68.017	N
23	P198	drag-coefficient-both-op	164.54	
24	P199	drag-airbody-op	32.763	N
25	[+] Water 4 and waves, 0 wind (F1)			
26	P200	drag-waterbody-op	23.182	N
27	P201	drag-coefficient-both-op	45.31	
28	P202	drag-airbody-op	4.5709	N
29	[+] Water 3 and waves, 10 wind (G1)			
30	P206	drag-waterbody-op	13.619	N
31	P207	drag-coefficient-both-op	27.681	
32	P208	drag-airbody-op	3.3356	N
33	[+] Open Channel 6 (H1)			
34	P188	drag-waterbody-op	51.116	N
35	P189	drag-coefficient-both-op	100.25	
36	P190	drag-airbody-op	10.288	N
37	[+] Open Channel 7 (I1)			
38	P191	drag-waterbody-op	68.513	N
39	P192	drag-coefficient-both-op	156.69	
40	P193	drag-airbody-op	27.457	N

B.3 Example of Post Processing Menu

